

Momentum reconstruction at the LHC for probing CP-violation in the stop sector

G. Moortgat-Pick^{a,c}, K. Rolbiecki^b, J. Tattersall^b

^a*II. Institut fuer Theoret. Physik, University of Hamburg, Luruper Chaussee 149,
D-22761 Hamburg, Germany*

^b*IPPP, University of Durham, Durham DH1 3LE, UK*

^c*DESY, Deutsches Elektronen-Synchrotron, Notkestr. 85, D-22607 Hamburg, Germany*

Abstract

We study the potential to observe CP-violating effects in SUSY \tilde{t}_1 -cascade decay chains at the LHC. Asymmetries composed by triple products of momenta of the final state particles are sensitive to CP-violating effects. Due to large boosts that dilute the asymmetries, these can be difficult to observe. If all particle masses in a cascade decay are known, it may be possible to reconstruct all momenta in the decay chains on an event-by-event basis even when we have missing momentum due to a stable LSP. After the reconstruction, the non-diluted CP-violating signal can be recovered and gets significantly enhanced so that an observation may become feasible. A fully hadronic study has been completed to define the areas of the mSUGRA parameter space that may yield a $3\text{-}\sigma$ observation with 500 fb^{-1} at the LHC.

e-mail:

`gudrid.moortgat-pick@desy.de`

`krzysztof.rolbiecki@durham.ac.uk`

`jamie.tattersall@durham.ac.uk`

Contents

| | | |
|----------|---|-----------|
| 1 | Introduction | 3 |
| 2 | Formalism | 5 |
| 2.1 | The process studied and the amplitude squared | 5 |
| 2.2 | Structure of the T-odd asymmetry | 6 |
| 3 | Momentum reconstruction | 8 |
| 3.1 | Dilution effects | 8 |
| 3.2 | Reconstruction procedure | 9 |
| 3.3 | Challenges from multiple solutions | 11 |
| 3.4 | Mass measurements | 11 |
| 4 | Parton level results | 12 |
| 4.1 | Chosen scenario: spectrum and decay modes | 12 |
| 4.2 | CP asymmetry at the parton level | 13 |
| 5 | Hadron level results | 14 |
| 5.1 | Cuts used and signal identification | 15 |
| 5.2 | Standard model background | 16 |
| 5.3 | Stop Production | 16 |
| 5.4 | Impact of momentum reconstruction on SUSY background separation . . . | 20 |
| 5.5 | Open experimental issues | 22 |
| 6 | Conclusions | 23 |
| A | Mixing in the stop sector | 24 |
| B | Mixing in the neutralino sector | 25 |
| C | Interaction Lagrangian and couplings | 26 |
| D | Amplitude squared including full spin correlations | 26 |
| D.1 | Neutralino production $\tilde{t}_1 \rightarrow \tilde{\chi}_j^0 t$ | 26 |
| D.2 | Neutralino decay $\tilde{\chi}_2^0 \rightarrow \tilde{\ell}_R^+ \ell^-$ | 28 |
| D.3 | Top decay $t \rightarrow W^+ b$ | 28 |
| | References | 28 |

1 Introduction

The Minimal Supersymmetric Standard Model (MSSM) is a particularly compelling extension of the Standard Model, that may soon be explored at the Large Hadron Collider (LHC). It allows one to stabilize the hierarchy between the electroweak (EW) scale and the Planck scale and to naturally explain electroweak symmetry breaking (EWSB) by a radiative mechanism. The naturalness of the scale of electroweak symmetry breaking and the Higgs mass places a rough upper bound on the superpartner masses of several TeV and the fits to the electroweak precision data point to a rather light SUSY spectrum [1]. If supersymmetry is discovered, many studies will be required to determine the exact details of its realisation. One of the interesting issues in this context is CP violation. While the observed amount of CP violation in the K and B sectors can be accommodated within the SM, another piece of evidence, the baryon asymmetry of the universe, requires a new source of CP violation [2–4].

The MSSM contains 105 free parameters [5] and a large number of these may have non-zero CP-violating phases, see e.g. [6]. Many of the phases are unphysical in the sense that they can be rotated away by a redefinition of the fields. The parameters normally chosen to be complex and relevant to this study are the U(1) and SU(3) gaugino mass parameters M_1 and M_3 , the higgsino mass parameter μ and the trilinear couplings of the third generation sfermions A_f ($f = b, t, \tau$). Hence we have,

$$M_1 = |M_1|e^{i\phi_1}, \quad M_3 = |M_3|e^{i\phi_3}, \quad \mu = |\mu|e^{i\phi_\mu}, \quad A_f = |A_f|e^{i\phi_{A_f}}. \quad (1)$$

The two complex parameters that enter the \tilde{t} sector at tree level are A_t and μ and in the $\tilde{\chi}_i^0$ sector μ and ϕ_{M_1} . Certain combinations of the CP-violating phases of these parameters are constrained by the experimental upper bounds on various electric dipole moments (EDMs), see e.g. [7]. Ignoring possible cancellations, the most severely constrained phase is that of μ which contributes to the EDMs at the one-loop level. In general for $\mathcal{O}(100)$ GeV masses, $|\phi_\mu|$ has to be very small and we therefore set $\phi_\mu = 0$ throughout our study. The phase of A_t has weaker constraints as it only contributes to the EDMs at the two loop level [8–14]. Here we study the complete range of ϕ_{A_t} in order to see the general dependencies exhibited by our observables and the luminosity required to observe this within the LHC environment. In principle, ϕ_{M_1} can also contribute to our observables but in the mSUGRA scenarios discussed in this paper, the dependence is weak due to the wino character of the $\tilde{\chi}_2^0$. We would like to stress that in the chosen scenario experimental bounds from EDMs can be evaded by arranging cancellations between various supersymmetric contributions for any value of A_t [7, 15–17].

In general CP phases alter the couplings and masses of SUSY particles, see [18] for a recent review at the LHC. Therefore, in principle we could detect CP-violating effects by studying mass spectra, cross sections or branching ratios [19, 20]. However, all of these observables are CP-even and can be faked by a multitude of other parameters. In addition, to make these measurements will require high precision and a good knowledge of the SUSY breaking mechanism.

In order to make the unambiguous observation of a complex parameter, we need to use CP-odd observables. Examples of CP-odd observables include rate asymmetries of cross sections and branching ratios. Another possibility, however, are observables that

are odd under T-transformations. Applying CPT-invariance, T-odd observables can be transferred under certain conditions into CP-odd variables, see Sec. 2.2. These kinds of observables can be defined using the triple product correlations of momenta that are based on spin correlations of particles, see [21, 22] for a recent review. For the case of SUSY at the LHC, we can do this using the final state particles of cascade decays.

The investigation of triple product correlations within SUSY at the LHC has been looked at for various different processes. \tilde{t} decays have been studied both in three-body [23–25] and two-body cascade decays [17, 26]. \tilde{b} decays have also been looked at in similar studies for two body cascade decays [27, 28]. In [29] we looked at $\tilde{q}\tilde{g}$ production and decay and studied how to cope with statistical limitations and dilution factors in searching for CP-phases in SUSY at the LHC. For the present paper, we extend the ideas described in detail in [29] of momentum reconstruction to \tilde{t} production and two-body decays. We further include hadronic, combinatorial and background effects to study whether CP-violation will be observable in the \tilde{t} sector at the LHC.

Specifically, we consider the LHC production process,

$$pp \rightarrow \tilde{t}_1 \tilde{t}_1^*. \quad (2)$$

Our signal CP-odd observable is then generated in the following two body decays,

$$\tilde{t}_1 \rightarrow \tilde{\chi}_2^0 t, \quad \tilde{\chi}_2^0 \rightarrow \tilde{\ell} \ell_N, \quad \tilde{\ell} \rightarrow \tilde{\chi}_1^0 \ell_F, \quad t \rightarrow b + W. \quad (3)$$

where ℓ_N and ℓ_F denote the near and far leptons respectively.

The CP-odd observables are then built from triple products of final state or reconstructable particles, e.g. $\vec{p}_{\ell_N} \cdot (\vec{p}_t \times \vec{p}_W)$.

Triple products constructed in this way are not Lorentz invariant but instead depend on the intrinsic boost of the produced particle in the laboratory frame. The observed asymmetry is maximal when the decay is at rest in the laboratory frame and any boost dilutes the observable. Consequently, we decide to use the idea of momentum reconstruction to find the momentum of the invisible $\tilde{\chi}_1^0$. We are able to perform momentum reconstruction for the decay chain shown in Eq. (3) as we have four on-shell mass conditions which we can solve for the four unknowns of the $\tilde{\chi}_1^0$ momentum on event-by-event basis. Once the $\tilde{\chi}_1^0$ momentum is known, we can find the rest frame of any particle involved in the decay chain and thus measure the maximum CP asymmetry.

An important note to make is that the sign of the asymmetry generated by the triple product flips if we consider the decay of the charge conjugate \tilde{t}_1^* . Therefore, in addition to measuring the triple product we must also determine the charge of the decaying \tilde{t}_1 . Unfortunately we cannot use a leptonically decaying W in this study as we must fully measure the t momentum to perform momentum reconstruction. Hence, we rely on the opposite \tilde{t}_1 decay to a single charged lepton final state to tag the charge of both produced stops e.g. $\tilde{t}_1^* \rightarrow \tilde{\chi}_1^0 \bar{t}, \bar{t} \rightarrow b \ell^- \nu_\ell$. As an aside, charge identification of the process is also required to rule out T_N -odd observables that can in principle be generated by final state interactions at the one-loop level [30], see Sec. 2.2 for more details. We compare the signal process with the charge-conjugated decay and if a non-zero asymmetry is observed in the combination, it must correspond to a violation of CP symmetry.

We begin in Sec. 2 by describing the process and underlying structure to derive the various triple products that can be formed. In Sec. 3 we move on to discuss the momentum reconstruction method and its application to the process studied. Sec. 4 gives the analytical results of the asymmetries at parton level. Hadron level results are described in Sec. 5 where we also discuss the effects of standard model and SUSY backgrounds. We also find that the method of momentum reconstruction significantly improves the signal to background ratio.

2 Formalism

2.1 The process studied and the amplitude squared

At the LHC, the light stop (\tilde{t}_1) particles can be produced via pair production,

$$pp \rightarrow \tilde{t}_1 \tilde{t}_1^* \quad (4)$$

In our study the CP-violating observables are produced in the following decay,

$$\tilde{t}_1 \rightarrow \tilde{\chi}_2^0 + t. \quad (5)$$

We require the $\tilde{\chi}_2^0$ to decay via two, 2-body leptonic channels,

$$\tilde{\chi}_2^0 \rightarrow \tilde{\ell}_R^\pm \ell_N^\mp \rightarrow \tilde{\chi}_1^0 \ell_N^\mp \ell_F^\pm, \quad (6)$$

where N and F denote the near and far leptons respectively. In addition, we only consider events where the t is fully reconstructable and hence decays hadronically,

$$t \rightarrow Wb \rightarrow q_u \bar{q}_d b. \quad (7)$$

Using the formalism of [31, 32], the squared amplitude $|T|^2$ of the full process can be factorised into the processes of production $gg \rightarrow \tilde{t}_1 \tilde{t}_1^*$ and the subsequent decays $\tilde{t}_1 \rightarrow t \tilde{\chi}_2^0$, $\tilde{\chi}_2^0 \rightarrow \tilde{\ell} \ell_N$, $\tilde{\ell} \rightarrow \tilde{\chi}_1^0 \ell_F$ and $t \rightarrow Wb$. We apply the narrow-width approximation but include the full spin correlations for production and decay of the intermediate particles, \tilde{t}_1 , $\tilde{\chi}_2^0$, $\tilde{\ell}$ and t . The use of the narrow-width approximation is appropriate since the widths of the respective particles are much smaller than the masses in all cases. The squared amplitude can then be expressed in the form,

$$\begin{aligned} |T|^2 = & 4|\Delta(\tilde{t}_1)|^2 |\Delta(\tilde{\chi}_2^0)|^2 |\Delta(\tilde{\ell})|^2 |\Delta(t)|^2 P(\tilde{t}_1 \tilde{t}_1^*) \left\{ P(\tilde{\chi}_2^0 t) D(\tilde{\chi}_2^0) D(\tilde{\ell}) D(t) \right. \\ & + \sum_{a=1}^3 \Sigma_P^a(\tilde{\chi}_2^0) \Sigma_D^a(\tilde{\chi}_2^0) D(\tilde{\ell}) D(t) + \sum_{b=1}^3 \Sigma_P^b(t) \Sigma_D^b(t) D(\tilde{\chi}_2^0) D(\tilde{\ell}) \\ & \left. + \sum_{a,b=1}^3 \Sigma_P^{ab}(\tilde{\chi}_2^0 t) \Sigma_D^a(\tilde{\chi}_2^0) \Sigma_D^b(t) D(\tilde{\ell}) \right\}, \quad (8) \end{aligned}$$

where $a, b = 1, 2, 3$ refers to the polarisation states of the neutralino $\tilde{\chi}_i^0$ and top quark t . In addition,

- $\Delta(\tilde{t}_1)$, $\Delta(\tilde{\chi}_2^0)$, $\Delta(\tilde{\ell})$ and $\Delta(t)$ are the pseudo-propagators of the intermediate particles which lead to the factors $E_{\tilde{t}_1}/m_{\tilde{t}_1}\Gamma_{\tilde{t}_1}$, $E_{\tilde{\chi}_2^0}/m_{\tilde{\chi}_2^0}\Gamma_{\tilde{\chi}_2^0}$, $E_{\tilde{\ell}_R}/m_{\tilde{\ell}_R}\Gamma_{\tilde{\ell}_R}$ and $E_t/m_t\Gamma_t$ in the narrow-width approximation.
- $P(\tilde{t}_1\tilde{t}_1)$, $P(t\tilde{\chi}_2^0)$, $D(\tilde{\chi}_2^0)$, $D(\tilde{\ell})$ and $D(t)$ (Appendix D) are the terms in the production and decay that are independent of the spin of the decaying neutralino and top, whereas,
- $\Sigma_P^a(\tilde{\chi}_i^0)$, $\Sigma_P^b(t)$, $\Sigma_P^{ab}(\tilde{\chi}_2^0t)$ and $\Sigma_D^a(\tilde{\chi}_2^0)$, $\Sigma_D^b(t)$ (Appendix D) are the spin-dependent terms giving the correlations between production and decay of the $\tilde{\chi}_2^0$ and t . We follow the formalism and conventions described in [32].
- It must be noted that the slepton $\tilde{\ell}$ produces no spin correlation term in the amplitude since it is a scalar.

Explicit expressions are given in Appendix D.

2.2 Structure of the T-odd asymmetry

As shown in the CPT-theorem [33,34], relativistic quantum field theories with usual spin-statistics relations have to be invariant under a CPT-transformation. This invariance guarantees that the masses and also the total widths of particles and antiparticles are the same. Since a true T-transformation is anti-unitary, which exchanges the initial and the final states, it is useful to study 'naive' T_N -transformations for collider-based experiments. The definition of T_N -transformations is to apply T-transformations to the initial and final states but without interchanging them. The unitarity of the S-matrix leads in the absence of re-scattering effects (i.e. in leading order in perturbation theory, no FSI, no width effects) to a conservation of the scattering amplitude under a CPT_N -transformation [30].

It is therefore useful to categorise CP-violating observables into T_N -odd and T_N -even observables. CPT_N invariance implies that a T_N -odd observable is also CP-odd in the absence of re-scattering effects. However, in case re-scattering effects contribute, i.e. $CPT_N \neq CPT$ -invariance, a T_N -odd signal may be caused by such re-scattering effects and does not necessarily imply CP-violation.

For all our observables we require that we know the charge of the decaying \tilde{t}_1 and can therefore distinguish the particle and anti-particle. Hence we can combine the process with the charge-conjugated decay to make an unambiguous observation of CP-violation via T_N -odd observables.

In general, it is therefore important to classify all terms of the corresponding amplitude squared, eq.(8), with respect to their T_N -odd or T_N -even character. Only the products that contain a T_N -odd contribution will lead to CP-odd violating observables:

- The spin-independent terms introduced in the previous section, $P(\tilde{t}_1\tilde{t}_1)$, $P(t\tilde{\chi}_2^0)$, $D(\tilde{\chi}_2^0)$, $D(\tilde{\ell})$, $D(t)$ do not cause any T_N -odd terms.
- The spin-dependent terms, $\Sigma_P^a(\tilde{\chi}_i^0)$, $\Sigma_P^b(t)$, $\Sigma_P^{ab}(\tilde{\chi}_2^0t)$, $\Sigma_D^a(\tilde{\chi}_2^0)$, $\Sigma_D^b(t)$, however, often can be divided up into T_N -even and T_N -odd terms, depending on the processes studied. In our case, a sequence of 2-body decays, however, we can only split

$\Sigma_P^{ab}(\tilde{\chi}_2^0 t) = \Sigma_{P,even}^{ab}(\tilde{\chi}_2^0 t) + \Sigma_{P,odd}^{ab}(\tilde{\chi}_2^0 t)$, all other spin-dependent terms only lead to T_N -even terms¹.

- Therefore, the T_N -odd term in the amplitude is, $\sum_{a,b=1}^3 \Sigma_{P,odd}^{ab}(\tilde{\chi}_2^0 t) \Sigma_D^a(\tilde{\chi}_2^0) \Sigma_D^b(t) D(\tilde{\ell})$.

When we contract the spin indices of the t and $\tilde{\chi}_2^0$ and evaluate the T_N -odd contribution we find that the following covariant product appears in the amplitude,

$$\Sigma_{P,odd}^{ab}(\tilde{\chi}_2^0 t) \Sigma_D^a(\tilde{\chi}_2^0) \Sigma_D^b(t) \sim i \epsilon_{\mu\nu\rho\sigma} s^{a,\mu}(\tilde{\chi}_2^0) p_{\tilde{\chi}_2^0}^\nu s^{b,\rho}(t) p_t^\sigma \times (p_{\ell_N} s^a)(p_{[b,W]} s^b), \quad (9)$$

$$\sim i \epsilon_{\mu\nu\rho\sigma} p_{\tilde{\chi}_2^0}^\nu p_{\ell_N}^\mu p_W^\rho p_t^\sigma, \quad (10)$$

where $\Sigma_{P,odd}^{ab}$, $\Sigma_D^a(\tilde{\chi}_2^0)$ and $\Sigma_D^b(t)$ are given by Eq. (69), Eq. (73) and Eq. (75) respectively.

The above equation is multiplied by the imaginary part of the coupling, Eq. (71) that contain terms from both the \tilde{t} , Eq. (39), and $\tilde{\chi}^0$, Eq. (50), mixing matrices. Hence, any complex phases contained in those mixing matrices will yield CP-violating effects that can be seen in an observable that exploits the covariant product. We can now expand the Lorentz invariant covariant product in terms of the explicit energy and momentum components,

$$\begin{aligned} \epsilon_{\mu\nu\rho\sigma} p_{\tilde{\chi}_2^0}^\nu p_{\ell_N}^\mu p_W^\rho p_t^\sigma = & E_{\tilde{\chi}_2^0} \vec{p}_{\ell_N} \cdot (\vec{p}_W \times \vec{p}_t) + E_W \vec{p}_t \cdot (\vec{p}_{\tilde{\chi}_2^0} \times \vec{p}_{\ell_N}) \\ & - E_{\ell_N} \vec{p}_W \cdot (\vec{p}_t \times \vec{p}_{\tilde{\chi}_2^0}) - E_t \vec{p}_{\tilde{\chi}_2^0} \cdot (\vec{p}_{\ell_N} \times \vec{p}_W). \end{aligned} \quad (11)$$

The first term in Eq. (11) shows the CP sensitive triple product that can be measured from final state momenta. However, this triple product is not Lorentz invariant and consequently can vary in both magnitude and sign in different reference frames. If we are in the rest frame of the $\tilde{\chi}_2^0$ though,

$$\epsilon_{\mu\nu\rho\sigma} p_{\tilde{\chi}_2^0}^\mu p_{\ell_N}^\nu p_W^\rho p_t^\sigma \longrightarrow m_{\tilde{\chi}_2^0} \vec{p}_{\ell_N} \cdot (\vec{p}_W \times \vec{p}_t), \quad (12)$$

the resulting asymmetry, Eq. (15), is uniquely defined since all other terms of the covariant product vanish as $\vec{p}_{\tilde{\chi}_2^0} \rightarrow 0$.

Hence we see that triple products of momenta, can be used as T_N -odd observables. In this paper we find that the triple products most useful to study are,

$$\mathcal{T}_{\ell_N} = \vec{p}_{\ell_N} \cdot (\vec{p}_W \times \vec{p}_t), \quad (13)$$

$$\mathcal{T}_{\ell\ell} = \vec{p}_b \cdot (\vec{p}_{\ell^+} \times \vec{p}_{\ell^-}). \quad (14)$$

where ℓ^+ and ℓ^- are the two leptons produced in the $\tilde{\chi}_2^0$ cascade decay. For the triple product, Eq. (14), the identification of near and far leptons is not required as is explained at the end of this section.

The T-odd asymmetry is then defined as,

$$\mathcal{A}_T = \frac{N_{\mathcal{T}_+} - N_{\mathcal{T}_-}}{N_{\mathcal{T}_+} + N_{\mathcal{T}_-}} = \frac{\int \text{sign}\{\mathcal{T}_f\} |T|^2 d\text{lips}}{\int |T|^2 d\text{lips}}, \quad (15)$$

¹This is different if 3-body decays are studied, see [24]. In that case spin-dependent terms from both the production $\Sigma_P^{ab}(\tilde{\chi}_2^0 t)$ as well as from the 3-body decay $\Sigma_D^a(\tilde{\chi}_2^0)$ lead to CP-odd contributions

where $f = \ell_N$ or $\ell\ell$, $d\text{lips}$ denotes Lorentz invariant phase space and $N_{\mathcal{T}_+}$ ($N_{\mathcal{T}_-}$) are the numbers of events for which \mathcal{T} is positive (negative). The denominator in Eq. (15), $\int |T|^2 d\text{lips}$, is equal to the total cross section.

We then define,

$$\mathcal{A}_{\ell_N} = \mathcal{A}_T(\mathcal{T}_{\ell_N}), \quad \mathcal{A}_{\ell\ell} = \mathcal{A}_T(\mathcal{T}_{\ell\ell}), \quad (16)$$

where \mathcal{A}_{ℓ_N} is the asymmetry from the triple product \mathcal{T}_{ℓ_N} and $\mathcal{A}_{\ell\ell}$ is the asymmetry from the triple product $\mathcal{T}_{\ell\ell}$.

As stated above, whilst the covariant product is Lorentz invariant, the triple products are not. However, we can see that for the triple product in Eq.(13), the rest frame of the $\tilde{\chi}_2^0$ and the \tilde{t}_1 are equivalent since ($p_{\tilde{t}} = p_{\tilde{\chi}_2^0} + p_t$),

$$\epsilon_{\mu\nu\rho\sigma} p_{\tilde{\chi}_2^0}^\mu p_{\ell_N}^\nu p_W^\rho p_t^\sigma = \epsilon_{\mu\nu\rho\sigma} p_{\tilde{t}_1}^\mu p_{\ell_N}^\nu p_W^\rho p_t^\sigma. \quad (17)$$

For the triple product $\mathcal{T}_{\ell\ell}$, Eq. (14), the covariant product can be re-expressed in the following form (exploiting momentum conservation, $p_{\tilde{\chi}_2^0} = p_{\tilde{\ell}} + p_{\ell_N}$, $p_{\tilde{\ell}} = p_{\ell_F} + p_{\tilde{\chi}_1^0}$, $p_W = p_t + p_b$),

$$\epsilon_{\mu\nu\rho\sigma} p_{\tilde{\chi}_2^0}^\mu p_{\ell_N}^\nu p_W^\rho p_t^\sigma = \epsilon_{\mu\nu\rho\sigma} (p_{\ell_F} + p_{\tilde{\chi}_1^0})^\mu p_{\ell_N}^\nu p_W^\rho p_b^\sigma. \quad (18)$$

However we now see that we have effectively two covariant products, one which contains the momentum of the $\tilde{\chi}_1^0$. In general, triple products containing the momentum of the far lepton will be lower as the far lepton is not directly correlated with the spin of $\tilde{\chi}_2^0$. Nevertheless, we can exploit and maximise the triple products originating from Eq. (17) and Eq. (18), if we know the momentum of the unstable particles in the decay chain. This can be provided by the momentum reconstruction procedure described in the following section.

Changing the decaying \tilde{t}_1 to a \tilde{t}_1^* or changing the charge of the near lepton ℓ_N reverses the sign of the covariant product. Consequently we have to know the charge of both the \tilde{t}_1 and the ℓ_N otherwise any asymmetry will cancel. The charge of the \tilde{t}_1 can be found by demanding that the opposite cascade produces a single lepton and thus a tri-lepton final state. We distinguish the near and far leptons using the momentum reconstruction technique, Sec. 3. However if for some reason the leptons cannot be identified we can still use the triple product $\mathcal{T}_{\ell\ell}$, Eq. (14). No lepton distinction is required as exchanging the near and far leptons has an extra sign change that cancels the change produced by the charge exchange.

3 Momentum reconstruction

3.1 Dilution effects

The triple product that is constructed from momenta in the laboratory frame suffers from dilution factors (~ 4) at the LHC. This is due to the lab frame being boosted with respect to the rest frame of the $\tilde{\chi}_2^0$ or \tilde{t}_1 , see Eq. (17), for a more detailed discussion see [24]. It results in a considerable reduction in the maximum asymmetry observable

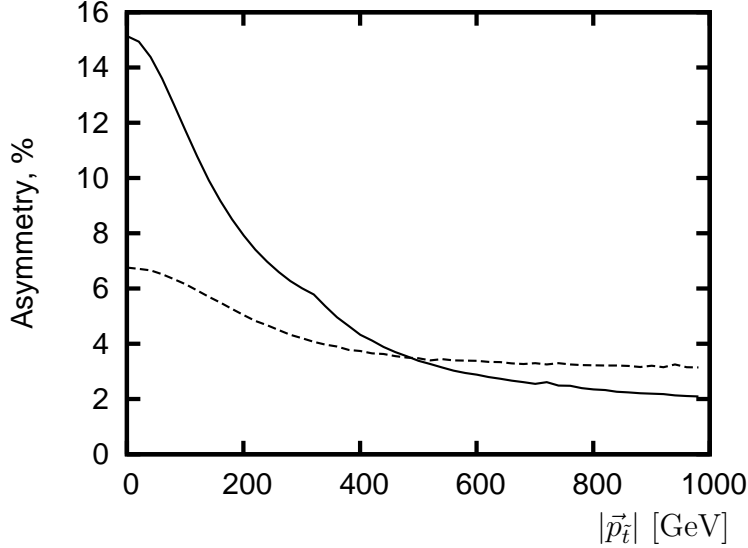


Figure 1: The asymmetry \mathcal{A}_T , Eq. (15), as a function of the stop momentum, $|\vec{p}_{\tilde{t}}|$, in the laboratory frame. The solid line is the asymmetry for the triple product \mathcal{T}_{ℓ_N} , Eq. (13) and the dotted line is for the triple product $\mathcal{T}_{\ell\ell}$, Eq. (14). The respective masses are given in Tab. 2, Tab. 3 and Tab. 4.

when we introduce the PDFs which causes an undetermined boost to the system. Fig. 1 shows how the asymmetry is diluted in the laboratory frame when we produce the \tilde{t}_1 with varying initial momenta. If we were able to reconstruct the momentum of the \tilde{t}_1 , we could perform a Lorentz transformation of all the momenta in the triple product into the \tilde{t}_1 rest frame and potentially recover the full asymmetry.

3.2 Reconstruction procedure

We are able to reconstruct the $\tilde{\chi}_1^0$ four momentum by reconstructing the following two body decay chain in full,

$$\tilde{t} \rightarrow t + \tilde{\chi}_2^0 \rightarrow t + \tilde{\ell}^\pm + \ell_N^\mp \rightarrow t + \tilde{\chi}_1^0 + \ell_N^\mp + \ell_F^\pm. \quad (19)$$

Assuming that all the masses in the decay chains are known, the kinematics can be fully reconstructed using the set of invariant mass conditions,

$$m_{\tilde{\chi}_1^0}^2 = (p_{\tilde{\chi}_1^0})^2, \quad (20)$$

$$m_{\tilde{\ell}^\pm}^2 = (p_{\tilde{\chi}_1^0} + p_{\ell_F^\pm})^2, \quad (21)$$

$$m_{\tilde{\chi}_2^0}^2 = (p_{\tilde{\ell}^\pm} + p_{\ell_N^\mp})^2 = (p_{\tilde{\chi}_1^0} + p_{\ell_F^\pm} + p_{\ell_N^\mp})^2, \quad (22)$$

$$m_{\tilde{t}_1}^2 = (p_{\tilde{\chi}_2^0} + p_t)^2 = (p_{\tilde{\chi}_1^0} + p_{\ell_F^\pm} + p_{\ell_N^\mp} + p_t)^2, \quad (23)$$

where p denote the four momenta of the respective particles.

We see that with the four equations we have enough information to solve the system and find each component of the $\tilde{\chi}_1^0$ four momentum. A solution to the above set of

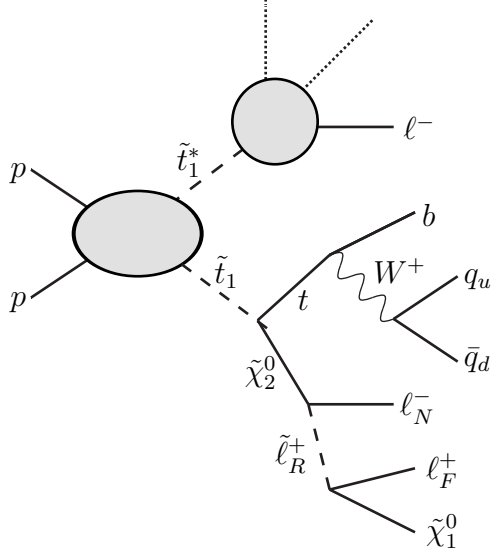


Figure 2: The process studied for momentum reconstruction.

equations is presented in [35] and we outline the procedure here. We first expand the $\tilde{\chi}_1^0$ momentum in terms of the final state momentum of the ℓ_F^\mp , ℓ_N^\pm and t ,

$$\vec{p}_{\tilde{\chi}_1^0} = a \vec{p}_{\ell_F^\pm} + b \vec{p}_{\ell_N^\mp} + c \vec{p}_t. \quad (24)$$

In order to derive a system of 3 linear equations for the unknowns $a - c$, we calculate $\vec{p}_{\tilde{\chi}_1^0} \cdot \vec{p}_{\ell_F^\pm}$, $\vec{p}_{\tilde{\chi}_1^0} \cdot \vec{p}_{\ell_N^\mp}$ and $\vec{p}_{\tilde{\chi}_1^0} \cdot \vec{p}_t$. Inserting Eq. (24) and exploiting Eqs. (21-23) we form the system of equations,

$$\mathcal{M} \begin{pmatrix} a \\ b \\ c \end{pmatrix} = \begin{pmatrix} \frac{1}{2}(m_{\tilde{\chi}_1^0}^2 - m_\ell^2) + E_{\tilde{\chi}_1^0} E_{\ell_F} \\ \frac{1}{2}(m_\ell^2 - m_{\tilde{\chi}_2^0}^2) + p_{\ell_F} \cdot p_{\ell_N} + E_{\tilde{\chi}_1^0} E_{\ell_N} \\ \frac{1}{2}(m_{\tilde{\chi}_2^0}^2 + m_t^2 - m_{\tilde{t}_1}^2) + p_{\ell_F} \cdot p_t + p_{\ell_N} \cdot p_t + E_{\tilde{\chi}_1^0} E_t \end{pmatrix}, \quad (25)$$

where,

$$\mathcal{M} = \begin{pmatrix} \vec{p}_{\ell_F} \cdot \vec{p}_{\ell_F} & \vec{p}_{\ell_F} \cdot \vec{p}_{\ell_N} & \vec{p}_{\ell_F} \cdot \vec{p}_t \\ \vec{p}_{\ell_N} \cdot \vec{p}_{\ell_F} & \vec{p}_{\ell_N} \cdot \vec{p}_{\ell_N} & \vec{p}_{\ell_N} \cdot \vec{p}_t \\ \vec{p}_t \cdot \vec{p}_{\ell_F} & \vec{p}_t \cdot \vec{p}_{\ell_N} & \vec{p}_t \cdot \vec{p}_t \end{pmatrix}. \quad (26)$$

We invert the matrix \mathcal{M} to find solutions for a , b and c in terms of constants and $E_{\tilde{\chi}_1^0}$. The on shell mass condition for the $\tilde{\chi}_1^0$, Eq. (20), can then be expressed as,

$$E_{\tilde{\chi}_1^0}^2 = (a, b, c) \mathcal{M} \begin{pmatrix} a \\ b \\ c \end{pmatrix} + m_{\tilde{\chi}_1^0}^2. \quad (27)$$

We solve the above quadratic, to find two solutions for $E_{\tilde{\chi}_1^0}$. These solutions are then substituted back into Eq. (24) to find all components of the \tilde{t}_1 momentum on an event-by-event basis.

3.3 Challenges from multiple solutions

We encounter a complication in the reconstruction as Eq. (20) is quadratic in $(p_{\tilde{\chi}_1^0})$. Consequently we have two solutions for $(p_{\tilde{\chi}_1^0})$ for each reconstructed event but we have no extra information in the single decay chain to determine which solution is physically correct. As we cannot distinguish which of these solutions corresponds to the physically correct configuration, we need to analyse both. Therefore, we calculate the \tilde{t}_1 momentum for both configurations and boost all final state particles in the triple product into the reconstructed \tilde{t}_1 rest frame. If the sign of both triple products are the same then the event is recorded but if the sign of the triple products are different, we discard the event since we cannot know which of the reconstructed solutions is correct. The method has the disadvantage that we lose events and therefore statistical significance. However, we find that the asymmetry can actually rise ($\approx 1.5\%$) as most of the events removed have small triple products and events with a small triple product lead to smaller asymmetries.

When performing the momentum reconstruction at the LHC we have additional problems from multiple solutions that come from combinatorial effects in the event. Firstly, to complete the reconstruction we need to correctly identify the near and far lepton in the decay chain Eq. (19) if we wish to compute the triple product \mathcal{T}_{ℓ_N} , Eq. (13) (although this information is not required for the triple product $\mathcal{T}_{\ell\ell}$, Eq. (14)). We find that in $\approx 20\%$ of events the wrong assignment of near and far leptons satisfy the kinematic equations Eq. (20)-(23) and produce two extra solutions for the momentum of the $\tilde{\chi}_1^0$ in addition to the solutions found from the correct configuration. In addition, we always require a third lepton in the event coming from the opposite decay chain to correctly identify the stop charge. For example the lepton produced in the decay chain $\tilde{t}_1^* \rightarrow \tilde{\chi}^- \bar{b}$, $\tilde{\chi}^- \rightarrow \ell^- + X$, where X are other neutral decay products. If this lepton is of the same flavour as those in the triple product decay chain there is a small chance that it can also reconstruct the $\tilde{\chi}_2^0$. All of these combinatorial issues are removed by again demanding that all calculated triple products are of the same sign and discarding any events where opposite sign solutions occur.

Further combinatorial issues occur with the reconstructed top in the event. Firstly a second b is always present in the opposite decay chain and this can occasionally combine with a reconstructed W to give a fake t . The opposite decay chain also can contain extra quarks that can produce more reconstructed t 's. Finally, the parton shower can sometimes radiate hard gluons that are also seen as extra jets and further complicate the combinatorial problem. Whenever extra t quarks are found that satisfy the event kinematics we perform the same procedure as for combinatorial leptons. Triple products are calculated for all reconstructed rest frames and only events, that yield the same sign for all the reconstructed triple products, are recorded.

3.4 Mass measurements

As mentioned above, we assume that the masses of all the SUSY particles in the decay chain will be known. However, for the majority of our equations in Eq. (25), we actually require the difference between various m^2 's in the decay chains and not the absolute mass. At the LHC, the most established way of measuring the SUSY spectrum is via mass end-

| Parameter | m_0 | $m_{1/2}$ | $\tan \beta$ | $\text{sign}(\mu)$ | A_0 |
|-----------|-------|-----------|--------------|--------------------|-------|
| Value | 65 | 210 | 5 | + | 0 |

Table 1: mSUGRA benchmark scenario (masses in GeV).

points ([36] and references therein) and this method will measure these mass differences with high accuracy $\mathcal{O}(1\%)$.

The on-shell mass condition for the $\tilde{\chi}_1^0$ requires the absolute mass scale and this should be measured at the LHC to a precision of better than 10% [36] for low mass scenarios similar to the phenomenology presented in this paper. As an extra check on the numerical stability of the reconstruction procedure, up to 20 GeV absolute mass errors were tested on the absolute mass scale of the decay chain as a conservative estimate. This had a negligible effect on the reconstruction efficiency and the CP-asymmetry and is therefore not considered to be a problem. In addition new methods have been proposed for measuring the sparticle masses from the kinematic invariants directly [35, 37–41]. These methods also use the mass invariants on an event-by-event basis but use this information to reconstruct the masses of the particles in the decay chain. Therefore, these methods are directly measuring the inputs we require for Eq. (20) and Eq. (25). We then use the output from these methods to reconstruct the $\tilde{\chi}_1^0$ on an event-by-event basis. Reviews of all the major mass reconstruction methods proposed for the LHC are given in [42, 43].

4 Parton level results

In this section we analyse numerically the CP-asymmetry at the parton level, with the inclusion of parton distribution functions, whilst in Sec. 5 we complete a hadronic level study to estimate the realistic environment and the discovery potential at the LHC. In particular, we focus on a specific mSUGRA parameter point, Tab. 1, at the parton level before discussing more general low mass mSUGRA scenarios for our hadronic study.

4.1 Chosen scenario: spectrum and decay modes

We choose for this study the mSUGRA scenario shown in Tab. 1 with an added CP-phase to the trilinear coupling ϕ_{A_t} . The spectrum at the electroweak scale have been derived using the RGE code `SPheno 2.2.3` [44] and the masses of the gauginos and scalars are shown in Tab. 2, Tab. 3 and Tab. 4 respectively. Using the low energy soft SUSY breaking parameters and the phase of the trilinear coupling ϕ_{A_t} , we calculate the masses and mixing of the \tilde{t}_i 's, see Appendix A for details.

For the presented analysis to work, we require the SUSY spectrum to have the following mass hierarchy,

$$m_{\tilde{t}_1} + m_t > m_{\tilde{\chi}_2^0} > m_{\tilde{\ell}_R^\pm} > m_{\tilde{\chi}_1^0}, \quad (28)$$

to allow for full momentum reconstruction. This hierarchy is often a feature in the

| Particle | $m_{\tilde{\chi}_1^0}$ | $m_{\tilde{\chi}_2^0}$ | $m_{\tilde{\chi}_3^0}$ | $m_{\tilde{\chi}_4^0}$ | $m_{\tilde{\chi}_1^\pm}$ | $m_{\tilde{\chi}_2^\pm}$ | $m_{\tilde{g}}$ |
|-----------|------------------------|------------------------|------------------------|------------------------|--------------------------|--------------------------|-----------------|
| Mass(GeV) | 77.7 | 142.4 | 305.1 | 330.3 | 140.7 | 329.9 | 514.116 |

Table 2: Masses (in GeV) of the gauginos calculated by **SPheno 2.2.3** [44].

| Particle | $m_{\tilde{t}_1}$ | $m_{\tilde{t}_2}$ | $m_{\tilde{b}_1}$ | $m_{\tilde{b}_2}$ | $m_{\tilde{q}_{dL}}$ | $m_{\tilde{q}_{dR}}$ | $m_{\tilde{q}_{uL}}$ | $m_{\tilde{q}_{uR}}$ |
|-----------|-------------------|-------------------|-------------------|-------------------|----------------------|----------------------|----------------------|----------------------|
| Mass(GeV) | 345.7 | 497.8 | 443.4 | 466.0 | 484.7 | 465.2 | 478.7 | 464.9 |

Table 3: Masses (in GeV) of the SUSY squarks calculated by **SPheno 2.2.3** [44] except for \tilde{t}_i that were calculated at tree level with phase $\phi_{A_t} = |\frac{4}{5}\pi|$.

| Particle | $m_{\tilde{\ell}_L}$ | $m_{\tilde{\ell}_R}$ | $m_{\tilde{\tau}_2}$ | $m_{\tilde{\tau}_1}$ |
|-----------|----------------------|----------------------|----------------------|----------------------|
| Mass(GeV) | 163.4 | 110.8 | 164.9 | 108.0 |

Table 4: Masses (in GeV) of the SUSY sleptons calculated by **SPheno 2.2.3** [44].

mSUGRA parameter space. In addition we concentrate on light mass scenarios as the study is statistically limited and consequently we require a large production cross section.

The feasibility of the study at the LHC depends heavily on the integrated luminosity. For this reason we look closely at the predicted cross section of the asymmetry decay chain,

$$\sigma = \sigma(pp \rightarrow \tilde{t}_1 \tilde{t}_1^*) \times BR(\tilde{t}_1 \rightarrow t \tilde{\chi}_2^0) \times BR(\tilde{\chi}_2^0 \rightarrow \tilde{\ell}^\pm \ell^\mp) \times BR(\tilde{\ell}^\pm \rightarrow \tilde{\chi}_1^0 \ell^\pm) \times BR(t \rightarrow q_u \bar{q}_d b), \quad (29)$$

and the relevant values for our scenario are shown in Tab. 5. In our study we also need to identify the charge of the \tilde{t}_1 in the opposite decay chain and this is possible when the decay products contain a single lepton (any number of jets are allowed). We see that the dominant production of single leptons from \tilde{t}_1 decays are via the channel $\tilde{t}_1 \rightarrow \tilde{\chi}_1^+ b$. However, as only the right sleptons and the bino-like $\tilde{\chi}_1^0$ are lighter than the wino-like $\tilde{\chi}_1^+$, the decay of the $\tilde{\chi}_1^+$ is via mixing terms or Yukawa couplings and hence the decay $BR(\tilde{\chi}_1^+ \rightarrow \tilde{\tau}_1^+ \nu_\tau)$ dominates, Tab. 5. For this reason we find that our study is far more promising if τ identification is possible and we compare results where τ identification has and has not been used later in the next section, Sec. 5.

4.2 CP asymmetry at the parton level

We start by discussing the dependence of ϕ_{A_t} on the parton level asymmetry, Eq. (15), for both the triple products $\mathcal{T}_{\ell N}$ and $\mathcal{T}_{\ell\ell}$, Eqs. (13), (14). In order to see the maximum dependence upon ϕ_{A_t} we reconstruct the \tilde{t}_1 at rest and calculate the triple product in this frame. It should be noted that the asymmetry is obviously a CP-odd quantity, Fig. 3.

| Parameter | Value |
|--|-------|
| $BR(\tilde{t}_1 \rightarrow \tilde{\chi}_1^0 t)$ | 34.6 |
| $BR(\tilde{t}_1 \rightarrow \tilde{\chi}_2^0 t)$ | 7.5 |
| $BR(\tilde{t}_1 \rightarrow \tilde{\chi}_1^+ b)$ | 50.1 |
| $BR(\tilde{t}_1 \rightarrow \tilde{\chi}_2^+ b)$ | 7.8 |
| $BR(\tilde{\chi}_2^0 \rightarrow \tilde{\mu}_R^+ \mu^- / \tilde{e}_R^+ e^-)$ | 11.6 |
| $BR(\tilde{\chi}_1^+ \rightarrow \tilde{\tau}_1^+ \nu_\tau)$ | 95.1 |
| $\sigma(pp \rightarrow \tilde{t}_1 \tilde{t}_1^*)$ [pb] | 3.44 |

Table 5: Nominal values of the branching ratios (in %) for various decays calculated in `Herwig++` [45, 46] with phase $\phi_{A_t} = |\frac{4}{5}\pi|$. In the last row, cross sections for stop pair production at the LHC with $\sqrt{s} = 14$ TeV at leading order (LO) from `Herwig++`.

We see from Fig. 3(a) that the largest asymmetry occurs for the triple product \mathcal{T}_{ℓ_N} , which attains $|\mathcal{A}_{\ell_N}|_{\max} \approx 15\%$ when $\phi_{A_t} \approx 0.8\pi$. For the triple product $\mathcal{T}_{\ell\ell}$, the asymmetry is smaller, $|\mathcal{A}_{\ell\ell}|_{\max} \approx 6.5\%$, because the ‘true’ CP triple product correlation is only partially measured, see Sec. 2.2.

If we now include the dominant production process at the LHC ($gg \rightarrow \tilde{t}_1 \tilde{t}_1^*$) and relevant parton distribution functions (MRST 2004LO [47]), we see that the asymmetries are significantly diluted, Fig. 3(b). The asymmetry for the triple product \mathcal{T}_{ℓ_N} , drops from $|\mathcal{A}_{\ell_N}|_{\max} \approx 15\%$ to $|\mathcal{A}_{\ell_N}|_{\max} \approx 4.5\%$ and the reduction is due to the boosted frame of the produced \tilde{t}_1 as discussed in Sec. 2.2. For the triple product $\mathcal{T}_{\ell\ell}$, the reduction in the asymmetry is far less, from $|\mathcal{A}_{\ell\ell}|_{\max} \approx 6.5\%$ to $|\mathcal{A}_{\ell\ell}|_{\max} \approx 3.8\%$. This is because the triple product, relies on the ℓ_F being correlated with the $\tilde{\ell}$ by the intrinsic boost of the $\tilde{\chi}_2^0, \tilde{\ell}$ system which already has a boost, even when the \tilde{t}_1 is at rest. As the \tilde{t}_1 becomes boosted, the boost of the $\tilde{\chi}_2^0, \tilde{\ell}$ system becomes proportionally less so, as the momentum of the \tilde{t}_1 is distributed throughout the decay chain. The difference in the dilution of the two asymmetries with \tilde{t} momentum can be seen in Fig. 1.

5 Hadron level results

In order to estimate the potential for observing CP-violating effects in \tilde{t}_1 decays at the LHC more realistically, we perform the analysis at the hadronic level. We use the `Herwig++` [45, 46] event generator to calculate all the matrix elements in the process, the initial hard interaction, the subsequent SUSY particle decays, the parton shower and the hadronisation. An important feature of `Herwig++` is that it calculates the spin correlations in the SUSY cascade decay and allows the input of complex mixing matrices. Consequently, the triple product CP-asymmetry can be automatically calculated within `Herwig++`.

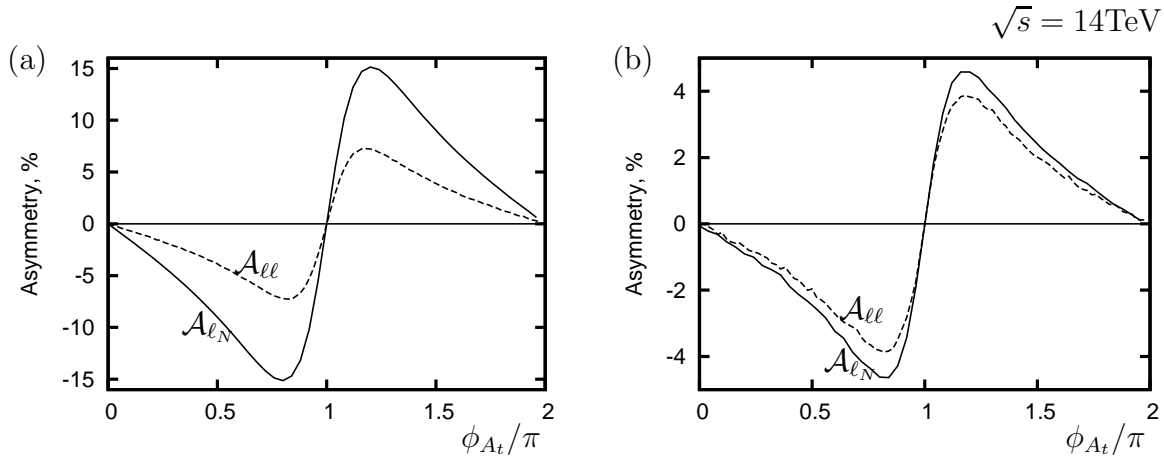


Figure 3: (a) The asymmetry \mathcal{A}_T , Eq. (15), in the rest frame of \tilde{t}_1 as a function of ϕ_{A_t} . (b) The asymmetry \mathcal{A}_T , Eq. (15), in the laboratory frame as a function of ϕ_{A_t} at the LHC at 14TeV. The solid line is the asymmetry for the triple product $\mathcal{T}_{\ell N}$, Eq. (13) and the dotted line is for the triple product $\mathcal{T}_{\ell\ell}$, Eq. (14).

5.1 Cuts used and signal identification

The hadronic analysis of the produced events has been performed within the program `Rivet` [48, 49]. We used the anti- k_t [50, 51] jet algorithm with $R=0.5$ and applied the following acceptance cuts,

- $p_{T\ell_i} > 10\text{GeV}$,
- $p_{Tj_i} > 20\text{GeV}$,
- invariant mass of opposite sign same flavour (OSSF) leptons: $M_{\ell^+\ell^-} > 10\text{GeV}$,
- $|\eta_{\ell_i}| < 2.5$,
- $|\eta_{j_i}| < 3.5$,
- lepton jet isolation, $\Delta R = 0.5$,
- b -tag efficiency = 60% [52],
- hadronic τ -tag efficiency (whenever used) = 40% [52].

To identify the events we demand three charged leptons in the final state, so that we can correctly identify the charge of each \tilde{t}_1 produced in the event, Sec. 2.2. In addition, we demand that a pair of these leptons are OSSF as is the case for light leptons from $\tilde{\chi}_2^0$ decay. Whenever a \tilde{t}_1 decays in our scenarios a b is produced and therefore we require at least one b -tag in the final state (in principle we could require 2 b -tags including the opposite decay chain but we loose 40% of events due to b -tagging efficiency). On top of the b we require at least 2 more jets to be found in the final state so the full reconstruction

of the t is possible. As all of our triple products and momentum reconstruction need a t we require at least one hadronic t to be reconstructed. For this procedure, we first demand that 2 jets (not b 's) reconstruct a W^\pm ($70\text{GeV} < M_{jj} < 90\text{GeV}$). We then impose that a reconstructed W^\pm and one b jet reconstruct a t ($150\text{GeV} < M_{W^\pm b} < 190\text{GeV}$).

Once these cuts have been passed we then perform the kinematical reconstruction shown in Sec. 3 with any t 's and OSSF leptons found in the final state. If the particles satisfy the kinematic constraints Eq. (20)-(23), we will have at least two different solutions on event-by-event basis for the momentum of the $\tilde{\chi}_1^0$. For each solution, the relevant rest frame triple product is calculated and only if all the signs of the triple products agree the event is accepted.

5.2 Standard model background

The following standard model backgrounds were produced with **Herwig++**: $t\bar{t}$, Drell-Yan gauge boson production (Z, γ, W), W +jet, Z +jet, WW , WZ , ZZ , $W\gamma$, WZ . In addition, we generate $t\bar{t}\ell^+\ell^-$ events with **MadGraph** [53] and then use **Herwig++** to perform the parton shower and hadronisation. We find that the only background to pass the event selection is $t\bar{t}\ell^+\ell^-$ with the very low rate of 0.03 events/ fb^{-1} after kinematical reconstruction. This corresponds to only $\approx 1\%$ of the signal process for our particular scenario.

Although the above result is encouraging, it must be stated that our analysis contains no jets mis-identified as leptons. As the standard model processes produced by **Herwig++** only contain a maximum of two hard leptons in the initial process, the lack of a trilepton signal is not surprising. However, we do not expect major problems from standard model backgrounds if we limit the study to leptons from the first and second generation. $t\bar{t}$ can be expected to provide the largest background when both W^\pm decay leptonically and an extra lepton is produced from a b or a mis-identified jet. Even when this occurs though, we still require an additional two hard jets in the event that have to combine with a b to form a t . Moreover, the final state then has to fulfil the reconstructed particular kinematics of our signal and finally all the calculated triple products have to agree.

To improve the statistical significance of our analysis, we also investigated the possibility of using τ -tagging in the opposite decay chain to that of our signal. In this analysis, we now change the original trilepton signal to a first or second lepton OSSF and additional hadronic τ . The mis-identification of a jet for a τ is much higher than for the other leptons and the standard model backgrounds may now become an issue [52]. However, this analysis is currently postponed to future studies.

5.3 Stop Production

We begin by studying $\tilde{t}_1\tilde{t}_1^*$ production along with the following decay chain,

$$\tilde{t}_1 \rightarrow \tilde{\chi}_2^0 t \rightarrow \tilde{\chi}_1^0 e^+ e^- j j b, \tag{30}$$

$$\tilde{t}_1^* \rightarrow \tilde{\chi}_1^0 \bar{t} \rightarrow \tilde{\chi}_1^0 \mu^- \bar{\nu}_\mu b. \tag{31}$$

to test the momentum reconstruction procedure. The above decay chain is the cleanest signal process from a combinatorial point of view. We find a reconstruction efficiency

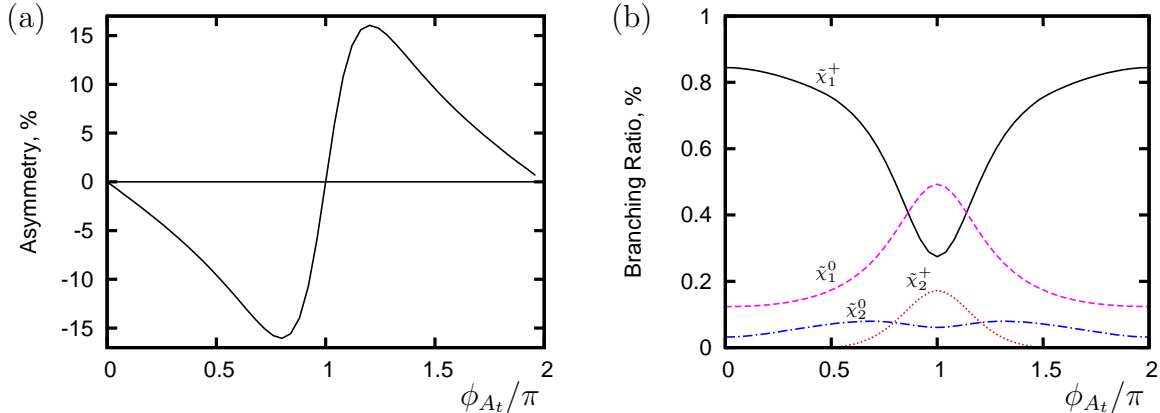


Figure 4: (a) The asymmetry \mathcal{A}_{ℓ_N} , Eq. (15), for the decay chain shown in Eq. (30)-(31) as a function of ϕ_{A_t} at the hadronic level after momentum reconstruction has been performed. (b) The branching ratios: $\tilde{t}_1 \rightarrow \tilde{\chi}_1^+ b$ (black solid), $\tilde{t}_1 \rightarrow \tilde{\chi}_2^+ b$ (red dotted), $\tilde{t}_1 \rightarrow \tilde{\chi}_1^0 t$ (purple slashed), $\tilde{t}_1 \rightarrow \tilde{\chi}_2^0 t$ (blue slash-dot).

of $\approx 5\%$ for this particular topology after cuts and the requirement for same sign triple products. The decay chain Eq. (31) has a single lepton in the final state allowing us to tag the charge of both the \tilde{t}_1 and \tilde{t}_1^* in the process.

For the CP-asymmetry, we now concentrate purely on the triple product \mathcal{T}_{ℓ_N} , Eq. (13) calculated in the reconstructed rest frame of the \tilde{t}_1 , as this is the observable with high significance at the LHC. Fig. 4(a) shows that there is virtually no dilution when we move to the hadronic level and the asymmetry stays at $|\mathcal{A}_{\ell_N}|_{\max} \approx 15\%$. In fact, the hadronic level reconstruction does induce a degree of dilution, $\approx 1.5\%$ but this is cancelled by our procedure of removing opposite sign triple products which enhances the asymmetry by a similar amount, Sec. 3.3.

In order to estimate whether it is possible to observe a CP-asymmetry in \tilde{t}_1 decays at the LHC we need to calculate the statistical significance of any result. We assume that $N_{\mathcal{T}_+}$ ($N_{\mathcal{T}_-}$), the numbers of events where \mathcal{T} is positive (negative) as in Eq. (15), are binomially distributed, giving the following statistical error [54],

$$\Delta(\mathcal{A}_T)^{\text{stat}} = 2\sqrt{\epsilon(1-\epsilon)/N}, \quad (32)$$

where $\epsilon = N_{\mathcal{T}_+}/(N_{\mathcal{T}_+} + N_{\mathcal{T}_-}) = \frac{1}{2}(1 + \mathcal{A}_T)$, and $N = N_{\mathcal{T}_+} + N_{\mathcal{T}_-}$ is the total number of events. Eq.(32) can be rearranged to give the required number of events for a desired significance.

The total cross section used to calculate the statistical significance of any result in this paper has been calculated using **Herwig++** at the leading order (LO) for consistency. However, next-to-leading order production cross sections are available and have been calculated using **Prospino** [55–57], cf. Tab. 6. We see that in general the cross sections at NLO are higher than those at LO suggesting that the effective luminosity at the LHC will be more optimistic than those shown in the following results. In addition, the

| | $\tilde{t}_1\tilde{t}_1^*$ | \tilde{g}, \tilde{q} |
|----------------------------------|----------------------------|------------------------|
| Herwig++ LO (pb ⁻¹) | 3.44 | 75.8 |
| Prospino LO (pb ⁻¹) | $3.34^{+1.15}_{-0.8}$ | $76.7^{+24.8}_{-17.3}$ |
| Prospino NLO (pb ⁻¹) | $5.04^{+1.19}_{-0.92}$ | $99.5^{+7.7}_{-9.6}$ |

Table 6: Cross section at the LHC with $\sqrt{s} = 14$ TeV production channel $\tilde{t}_1\tilde{t}_1^*$ and coloured SUSY production for both leading order (LO) and next-to-leading order (NLO). All cross sections were calculated using **Herwig++** [45,46] or **Prospino** [55–57]. The errors indicated next to the **Prospino** cross sections relate to varying the factorisation and renormalisation scales from $0.5m_{\tilde{t}_1} \rightarrow 2m_{\tilde{t}_1}$.

factorisation and renormalisation scale uncertainties are shown that indicates an estimate of the underlying theoretical uncertainty.

Due to the phase dependence of both the \tilde{t}_1 branching ratios, see Fig. 4(b), and production cross section, the statistical significance for different values of ϕ_{A_t} cannot be trivially extrapolated. The total number of events observed will be an interplay between the branching ratios and the production cross section. However, in the case of branching ratios, each of the decays, $\tilde{t}_1 \rightarrow \tilde{\chi}_1^+ b$, $\tilde{t}_1 \rightarrow \tilde{\chi}_2^+ b$ and $\tilde{t}_1 \rightarrow \tilde{\chi}_1^0 t$ has a different reconstruction efficiency and asymmetry dilution that needs to be calculated. For example, we see from Fig. 4(b) that the branching ratio for the decay $\tilde{t}_1 \rightarrow \tilde{\chi}_2^+ b$ increases noticeably as we vary ϕ_{A_t} from $\phi_{A_t} = 0$ to $\phi_{A_t} = |\pi|$ due to this decay becoming kinematically more favourable. The $\tilde{\chi}_2^+$ has a large number of final states with no lepton however, so consequently the number of signal events decreases. Also, the $\tilde{\chi}_2^+$ decays generally contain extra jets that make the reconstruction of the event more difficult and thus reduce the efficiency of this channel.

Fig. 5(a) shows the asymmetry when all \tilde{t}_1 decay channels are considered and an estimate of the amount of luminosity required for a 3σ -observation of a non-zero asymmetry for pure $\tilde{t}_1\tilde{t}_1^*$ production at the LHC. We can see that the asymmetry is slightly diluted when all \tilde{t}_1 decay modes are included from $|\mathcal{A}_{\ell_N}|_{\max} \approx 15\%$ to $|\mathcal{A}_{\ell_N}|_{\max} \approx 12.5\%$. The dilution is due to reconstructed events that are not originating from the signal process, Eq. (19). These events have no overall asymmetry and therefore simply dilute the signal. The horizontal lines show the estimate of the required luminosity required to see a certain asymmetry; an asymmetry can be seen at the 3σ level where the asymmetry curve in Fig. 5(a) lies outside the luminosity band. The luminosity bands are not flat because as discussed before, both the branching ratios and production cross section of the \tilde{t}_1 vary with the phase ϕ_{A_t} . We can see that in our scenario for pure $\tilde{t}_1\tilde{t}_1^*$ production, we expect a sensitivity for $|0.5\pi| < \phi_{A_t} < |0.9\pi|$ with 500 fb^{-1} .

We can see the effect of varying the mSUGRA parameters $\tan\beta$ and A_0 in Fig. 5(b). It is shown that as the value of either $\tan\beta$ or A_0 is increased, we require more luminosity to see a statistically significant observation even with maximum asymmetry. An increase in $\tan\beta$ decreases the sensitivity because the branching ratio $\tilde{\chi}_2^0 \rightarrow \tilde{\ell}^\pm \ell^\mp$ is reduced. The reduction is due to $\tilde{\tau}$'s becoming more mixed which increases the left handed component

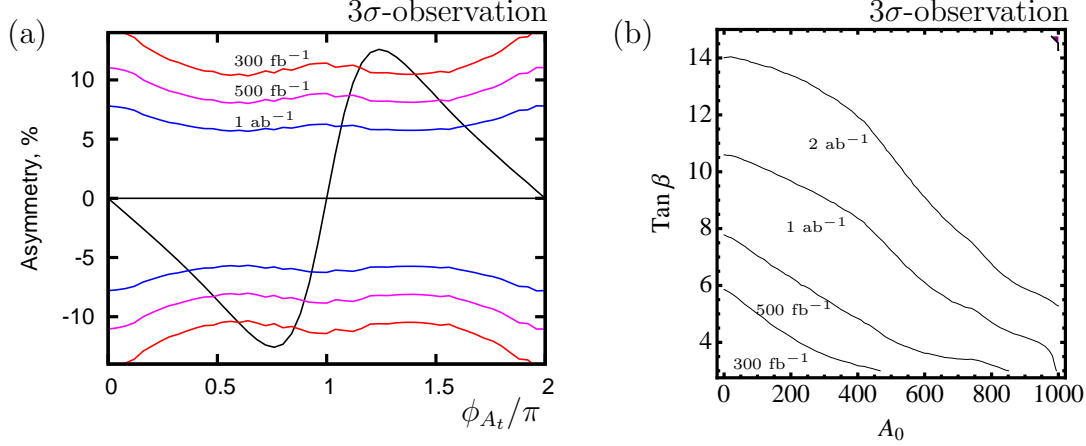


Figure 5: Pure $\tilde{t}_1\tilde{t}_1^*$ production, all decay channels included, see Tab. 5 for branching ratios for the specific parameter point and Fig. 4 for how these alter with ϕ_{A_t} . τ tagging is included in both plots. (a) Asymmetry, \mathcal{A}_{ℓ_N} , at reference point with 3σ -luminosity lines shown. (b) Minimum luminosity required for 3σ -discovery in $\tan\beta, A_0$ plane when asymmetry, \mathcal{A}_{ℓ_N} , is maximal.

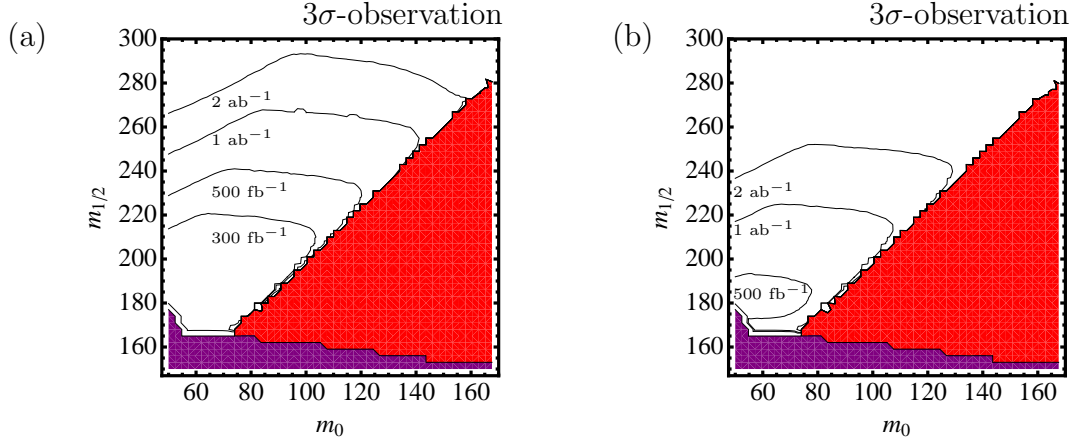


Figure 6: Minimum luminosity required for 3σ -discovery in $m_0, m_{1/2}$ plane when asymmetry, \mathcal{A}_{ℓ_N} , is maximal. Pure $\tilde{t}_1\tilde{t}_1^*$ production, all decay channels included, see Tab. 5 for branching ratios for the specific parameter point and Fig. 4 for how these alter with ϕ_{A_t} . Purple area is ruled out by LEP direct detection [58] and red area has no two body decay $\tilde{\chi}_2^0 \rightarrow \tilde{\ell}^\pm \ell^\mp$. (a) With τ tagging. (b) Without τ tagging.

in the lighter $\tilde{\tau}$. Therefore, the $\tilde{\tau}_1$ couples more strongly to the predominantly wino $\tilde{\chi}_2^0$ and begins to dominate this decay channel at the expense of the signal process. A rise in A_0 decreases sensitivity mainly because the CP-asymmetry is reduced. The reason is that after RGE running, an increase in A_0 reduces the magnitude of the trilinear coupling A_t that contains the phase, ϕ_{A_t} that we are interested in. Hence the CP effects are reduced.

Similarly, Fig. 6(a) shows the effect of varying the mSUGRA parameters m_0 and $m_{1/2}$ on the minimum luminosity required for an observation of CP effects. We note as general trend that as $m_{1/2}$ is increasing, we need more luminosity to observe the CP-violating triple products. This is due to the increase in \tilde{t}_1 mass which reduces the production cross

| | $\tilde{t}_1\tilde{t}_1^*$ | SUSY | $\tilde{t}_1\tilde{t}_1^*$ Signal / SUSY Background |
|---|----------------------------|-----------------|---|
| Cross Section (pb^{-1}) | 3.44 | 80.1 | |
| Events with 500 fb^{-1} | 1.7×10^6 | 4×10^7 | |
| Events with 500 fb^{-1} Initial selection | 32389 | 410735 | 0.079 |
| Events with 500 fb^{-1} Top Reconstruction | 7117 | 64729 | 0.11 |
| Events with 500 fb^{-1} Kinematic Reconstruction | 1213 | 3759 | 0.32 |
| Events with 500 fb^{-1} Extra SUSY cuts | 901 | 967 | 0.93 |

Table 7: Cross section, number of events and signal to background ratio at the LHC with $\sqrt{s} = 14 \text{ TeV}$ at LO for both the production channel $\tilde{t}_1\tilde{t}_1^*$ and inclusive SUSY production. All cross sections were calculated using `Herwig++` [45, 46].

section for $\tilde{t}_1\tilde{t}_1^*$. If we increase m_0 we see that a large area of the parameter space has no two body decay $\tilde{\chi}_2^0 \rightarrow \tilde{\ell}^\pm \ell^\mp$ as $\tilde{\ell}^\pm > \tilde{\chi}_2^0$.

Fig. 6(b) indicates the effect of having no hadronic τ -tagging for the decay $\tilde{\chi}_1^+ \rightarrow \tilde{\tau}_1^+ \nu_\tau$. The τ final state dominates the $\tilde{\chi}_1^+$ decay which in turn is the dominant product of the \tilde{t}_1 in low mass mSUGRA scenarios, Tab. 5. As stated in the beginning of Sec. 5 we assume a 40% τ -tagging efficiency and without this we lose approximately a factor of 2 in effective luminosity for our signal process.

5.4 Impact of momentum reconstruction on SUSY background separation

All of the previous sections results have assumed that the $\tilde{t}_1\tilde{t}_1^*$ process can be isolated effectively. However, in the mSUGRA scenarios investigated many other SUSY particles will be produced. Tab. 7 shows that the total production cross section for SUSY is ≈ 25 times greater than for $\tilde{t}_1\tilde{t}_1^*$ production and we can therefore expect sizable backgrounds. We can also expect that the vast majority of the SUSY background processes will have no other spin correlated CP-sensitive triple product with the same final state and will therefore just act as a dilution to the CP-asymmetry by contributing to the denominator of Eq. (15).

Tab. 7 shows that after the initial event selection and top reconstruction, the SUSY background is still ≈ 10 times larger than the signal process. Note that if we apply the kinematical reconstruction to these events we see that we substantially reduce the background to be only ≈ 3 times larger!

In order to observe CP-violating effects in $\tilde{t}_1\tilde{t}_1^*$ production at the LHC, however, the

signal to background ratio may still be too high and consequently we need further cuts to isolate the signal process. We notice that in mSUGRA scenarios, the largest background comes from \tilde{g} production followed by the dominant decay to either sbottom, $\tilde{g} \rightarrow \tilde{b}_i b$ with a branching ratio of $\approx 30\%$. The \tilde{b}_i decays dominantly to $\tilde{\chi}_2^0 b$ or $\tilde{\chi}_1^+ t$ which leads to a very similar final state as the signal process when combined with the opposite decay chain. The difference between the SUSY background and the \tilde{t}_1 's is that the \tilde{g} and first and second generation \tilde{q} have a higher mass. In addition, a gluino has in general one more decay vertex in the cascade decay producing another hard jet. These two factors mean that the average p_T of the particles produced in the event will be higher and the number of jets will be greater, thus we can use these characteristics to discriminate the signal from the background. Hence we cut on the number of jets reconstructed in an event,

$$\text{Number of jets} < 6. \tag{33}$$

For the p_T cuts, we have,

$$p_T(\text{Hardest Jet}) < 200 \text{ GeV}, \tag{34}$$

$$p_T(\text{2nd Jet}) < 130 \text{ GeV}, \tag{35}$$

$$p_T(\text{3rd Jet}) < 80 \text{ GeV (if applicable)}, \tag{36}$$

$$p_T(\text{Any } b \text{ Jet}) < 150 \text{ GeV}, \tag{37}$$

$$p_T(\text{Any Lepton}) < 100 \text{ GeV}. \tag{38}$$

Tab. 7 shows that after all these cuts are performed the signal to background ratio improves significantly and we now have roughly the same number of signal and background events in the sample.

If we now re-evaluate the luminosity plots with the SUSY background included, Fig. 7,8, we see that more luminosity is now required to observe a statistically significant effect. Due to the background dilution of the asymmetry, we now have $|\mathcal{A}_{\ell N}|_{\text{max}} \approx 6.5\%$ for our scenario Fig. 7. Consequently we are now only sensitive to phases between $|0.6\pi| < \phi_{A_t} < |0.85\pi|$ with 1 ab^{-1} of data. If we look at the $\tan\beta$, A_0 contour plot we see that sensitivity at the LHC for 1 ab^{-1} is only possible for small values of $\tan\beta$.

However, we would like to emphasise that it may be possible to substantially improve the statistical significance of an asymmetry measurement and return to close to the significance achieved when looking at a purely $\tilde{t}_1 \tilde{t}_1^*$ process, even with the same SUSY background. Namely, via measuring the SUSY spectra (in particular the \tilde{g} and \tilde{b}) a good estimate of the background should be possible. The background events can then be subtracted from the denominator of the asymmetry, Eq. (15), to give the true value of the asymmetry. Thus, the statistical significance should be much improved.

We would also like to remind the reader that this subtraction only becomes reliable if the signal to background ratio is good enough otherwise the signal is swamped by statistical fluctuations. Thus the momentum reconstruction procedure is vital since it significantly reduces the backgrounds that are present.

Similarly, a more constrained area of observability is seen in the m_0 , $m_{1/2}$ plane, Fig. 8(a). With 1 ab^{-1} of data, our study suggests that only if $m_{1/2} < 220 \text{ GeV}$ will it be possible to observe a CP-phase in the stop sector. Again, we see the importance of τ -tagging to our study from the difference between Fig. 8(a) and Fig. 8(b). If τ -tagging

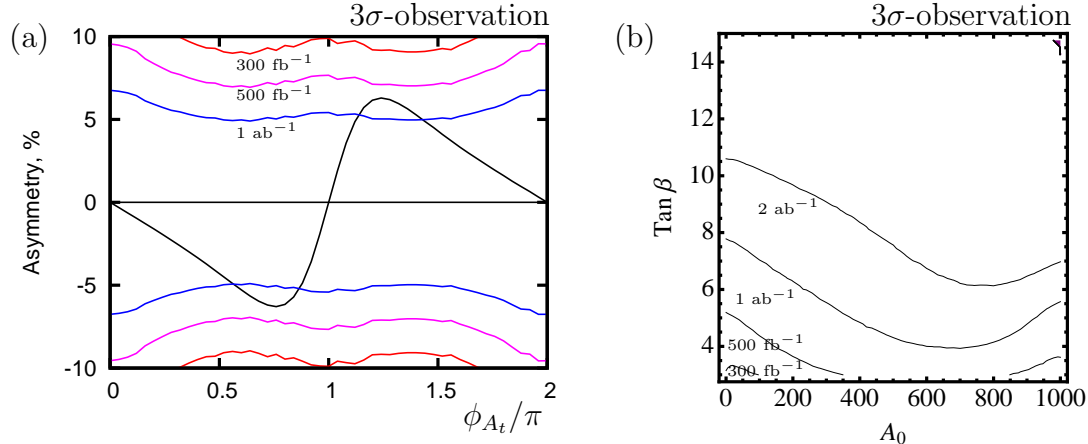


Figure 7: General SUSY production for the asymmetry \mathcal{A}_{ℓ_N} . τ tagging is included in both plots. (a) Asymmetry, \mathcal{A}_{ℓ_N} , at reference point with 3σ -luminosity lines shown. (b) Minimum luminosity required for 3σ -discovery in $\tan\beta, A_0$ plane when asymmetry, \mathcal{A}_{ℓ_N} , is maximal.

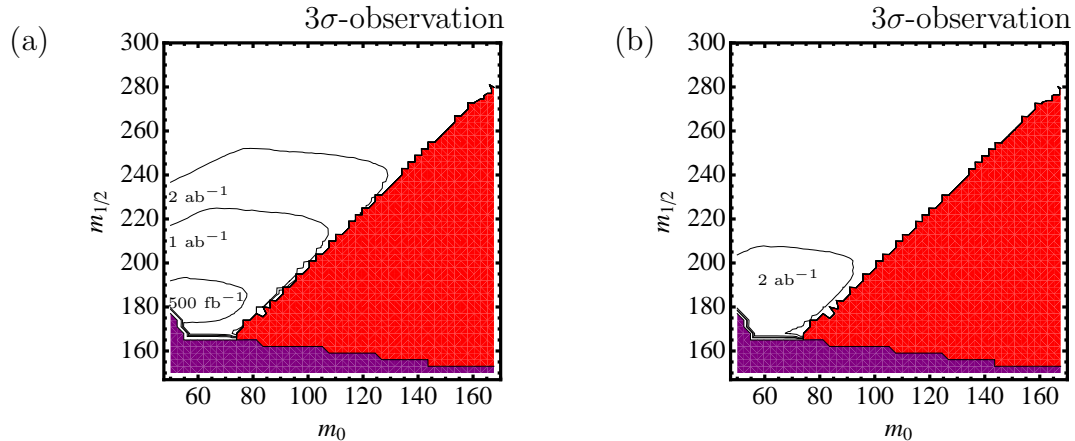


Figure 8: General SUSY production for the asymmetry \mathcal{A}_{ℓ_N} . Minimum luminosity required for 3σ -discovery in $m_0, m_{1/2}$ plane when asymmetry, \mathcal{A}_{ℓ_N} , is maximal. Purple area is ruled out by LEP direct detection [58] and red area has no two body decay $\tilde{\chi}_2^0 \rightarrow \tilde{\ell}^\pm \ell^\mp$. (a) With τ tagging. (b) Without τ tagging.

is not used in the study, no CP-violation in the \tilde{t}_1 sector can be observed with 1 ab^{-1} of data.

5.5 Open experimental issues

Although the presented study was completed at the hadronic level, a full detector simulation should be completed to confirm the conclusions of this paper. The most obvious experimental issue that could affect our results is the finite momentum resolution of the detector for both jets and leptons when performing momentum reconstruction. However, the resolution was tested with regards to momentum reconstruction in [29] with a significantly more complicated final state and it was found to have only a small effect.

In terms of background suppression the mis-tagging of various objects could increase both the standard model and SUSY background. For the standard model background, the most obvious example is the $t\bar{t}$ process generating a trilepton signal [52]. The process requires a jet to be mistagged as a lepton, which is not investigated in this study. The suitability of hadronic τ -tagging in the study also needs to be investigated thoroughly as these are expected to have significant mis-identification rates [52]. However, this is beyond the scope of this theoretical study.

6 Conclusions

In this paper we have investigated the problem of discovering CP-violating effects at the Large Hadron Collider. We studied $\tilde{t}_1\tilde{t}_1^*$ production and subsequent two body decays. Triple product correlations can be formed from the final state particles that are sensitive to the presence of complex phases in the model. Since triple products depend crucially on spin correlations and are therefore sensitive to CP-odd observables, they have been included both in the analytical calculation and the event generation, that has been performed using `Herwig++ 2.3.2`. The process of special interest in our case was the \tilde{t}_1 decay into t and $\tilde{\chi}_2^0$ followed by two, 2-body leptonic decays. For this decay in our mSUGRA scenario one can expect an asymmetry in the triple product distribution of up to 15% when calculated in the rest frame of the decaying neutralino. The source of the CP violation in our case was the phase of the trilinear coupling A_t that attains a value of $\phi_{A_t} \sim 0.8$ when the asymmetry is maximum in our scenario.

Due to the hadronic experimental environment of the LHC, precise measurements will be a challenge both from experimental and theoretical point of view. The rest frame CP-odd asymmetry is diluted by the high boosts of the produced particles and this makes an observation difficult. We studied the impact of momentum reconstruction of invisible LSPs to get access to the rest frame of the \tilde{t}_1 . Using a set of invariant kinematic conditions we showed that it is possible to fully reconstruct the production and decay process on an event-by-event basis. The reconstruction was performed on events including the parton shower and hadronisation. Having fully reconstructed events we are able to boost particle momenta back to the rest frame of the \tilde{t}_1 and the maximum asymmetry is recovered to 15%. In addition, momentum reconstruction leads to a significant increase in the signal background ratio and thus is very important in attempting to isolate the process of interest.

If we consider exclusive \tilde{t}_1 production and all possible \tilde{t}_1 decay chains the maximum asymmetry is diluted slightly to $\sim 12.5\%$. In the mSUGRA scenario considered in this paper one should expect to see a 3σ effect at $\mathcal{L} = 500 \text{ fb}^{-1}$ for phases in the range $|0.5\pi| \lesssim \phi_{A_t} \lesssim |0.9\pi|$. If general SUSY production is considered, significant backgrounds to our signal process are present and extra kinematical cuts are required to remove this background. Even after these cuts some SUSY background remains and our maximum asymmetry is reduced to $\sim 6.5\%$. To see a 3σ effect at the LHC would require $\mathcal{L} = 1 \text{ ab}^{-1}$ of data for sensitivity to phases in the range $|0.6\pi| \lesssim \phi_{A_t} \lesssim |0.85\pi|$.

We emphasise that the asymmetry after momentum reconstruction is a much cleaner observable from a theoretical point of view, thanks to a well defined final state. Therefore,

using the above technique provides prospects for the observation of CP-violating effects for a range of the phase ϕ_{A_t} after a few years of LHC running at the high luminosity. The full assessment of LHC’s ability to resolve CP violation in the MSSM, however, will definitely require a detailed simulation of detector effects, SM and SUSY backgrounds which is beyond the scope of the present phenomenological analysis. The promising results of this study may encourage such further simulations.

Acknowledgements

The authors wish to thank Peter Wienemann, Philip Bechtle, Björn Gosdzik and Frank Krauss for valuable discussions. We also are grateful to David Grellscheid and Peter Richardson for their assistance in the use of `Herwig++`. In addition we would like to thank Frank Siegert and Hendrik Hoeth for their help in the use of `Rivet`. KR is supported by the EU Network MRTN-CT-2006-035505 “Tools and Precision Calculations for Physics Discoveries at Colliders” (HEPTools). JT is supported by the UK Science and Technology Facilities Council (STFC).

Appendices

A Mixing in the stop sector

In the Minimal Supersymmetric Standard Model the stop sector is defined by the mass matrix $\mathcal{M}_{\tilde{t}}$ in the basis of gauge eigenstates $(\tilde{t}_L, \tilde{t}_R)$. The 2×2 mass matrix depends on the soft scalar masses $M_{\tilde{Q}}$ and $M_{\tilde{U}}$, the supersymmetric higgsino mass parameter μ , and the soft SUSY-breaking trilinear coupling A_t . It is given as

$$\mathcal{M}_{\tilde{t}}^2 = \begin{pmatrix} m_t^2 + m_{LL}^2 & m_{LR}^* m_t \\ m_{LR} m_t & m_t^2 + m_{RR}^2 \end{pmatrix}, \quad (39)$$

where

$$m_{LL}^2 = M_{\tilde{Q}}^2 + m_Z^2 \cos 2\beta \left(\frac{1}{2} - \frac{2}{3} \sin^2 \theta_W \right), \quad (40)$$

$$m_{RR}^2 = M_{\tilde{U}}^2 + \frac{2}{3} m_Z^2 \cos 2\beta \sin^2 \theta_W, \quad (41)$$

$$m_{LR} = A_t - \mu^* \cot \beta, \quad (42)$$

and $\tan \beta = v_2/v_1$ is the ratio of the vacuum expectation values of the two neutral Higgs fields which break the electroweak symmetry. From the above parameters only μ and A_t can take complex values

$$A_t = |A_t| e^{i\phi_t}, \quad \mu = |\mu| e^{i\phi_\mu}, \quad (0 \leq \phi_t, \phi_\mu < 2\pi), \quad (43)$$

thus yielding CP violation in the stop sector.

The hermitian matrix $\mathcal{M}_{\tilde{t}}^2$ is diagonalized by a unitary matrix $\mathcal{R}_{\tilde{t}}$,

$$\mathcal{R}_{\tilde{t}} \mathcal{M}_{\tilde{t}}^2 \mathcal{R}_{\tilde{t}}^\dagger = \begin{pmatrix} m_{\tilde{t}_1}^2 & 0 \\ 0 & m_{\tilde{t}_2}^2 \end{pmatrix}, \quad (44)$$

where we choose the convention $m_{\tilde{t}_1}^2 < m_{\tilde{t}_2}^2$ for the masses of \tilde{t}_1 and \tilde{t}_2 . The matrix $\mathcal{R}_{\tilde{t}}$ rotates the gauge eigenstates, \tilde{t}_L and \tilde{t}_R , into the mass eigenstates \tilde{t}_1 and \tilde{t}_2 as follows

$$\begin{pmatrix} \tilde{t}_1 \\ \tilde{t}_2 \end{pmatrix} = \mathcal{R}_{\tilde{t}} \begin{pmatrix} \tilde{t}_L \\ \tilde{t}_R \end{pmatrix} = \begin{pmatrix} \cos \theta_{\tilde{t}} & \sin \theta_{\tilde{t}} e^{-i\phi_{\tilde{t}}} \\ -\sin \theta_{\tilde{t}} e^{i\phi_{\tilde{t}}} & \cos \theta_{\tilde{t}} \end{pmatrix} \begin{pmatrix} \tilde{t}_L \\ \tilde{t}_R \end{pmatrix}, \quad (45)$$

where $\theta_{\tilde{t}}$ and $\phi_{\tilde{t}}$ are the mixing angle and the CP-violating phase of the stop sector, respectively. The masses are given by

$$m_{\tilde{t}_{1,2}} = \frac{1}{2} \left(2m_{\tilde{t}}^2 + m_{LL}^2 + m_{RR}^2 \mp \sqrt{(m_{LL}^2 - m_{RR}^2)^2 + 4|m_{LR}|^2 m_{\tilde{t}}^2} \right), \quad (46)$$

whereas for the mixing angle and the CP phase we have

$$\cos \theta_{\tilde{t}} = \frac{-m_t |m_{LR}|}{\sqrt{m_{\tilde{t}}^2 |m_{LR}|^2 + (m_{\tilde{t}_1}^2 - m_{LL}^2)^2}}, \quad (47)$$

$$\sin \theta_{\tilde{t}} = \frac{m_{LL}^2 - m_{\tilde{t}_1}^2}{\sqrt{m_{\tilde{t}}^2 |m_{LR}|^2 + (m_{\tilde{t}_1}^2 - m_{LL}^2)^2}}, \quad (48)$$

$$\phi_{\tilde{t}} = \arg(A_t - \mu^* \cot \beta). \quad (49)$$

By convention we take $0 \leq \theta_{\tilde{t}} < \pi$ and $0 \leq \phi_{\tilde{t}} < 2\pi$. It must be noted that $\phi_{\tilde{t}}$ is an ‘effective’ phase and does not directly correspond to the phase of any MSSM parameter. Instead, the phase will have contributions from both ϕ_{A_t} and ϕ_{μ} . However, in this study we set $\phi_{\mu} = 0$ due to the EDM constraints.

If $m_{LL} < m_{RR}$ then $\cos^2 \theta_{\tilde{t}} > \frac{1}{2}$ and \tilde{t}_1 has a predominantly left gauge character. On the other hand, if $m_{LL} > m_{RR}$ then $\cos^2 \theta_{\tilde{t}} < \frac{1}{2}$ and \tilde{t}_1 has a predominantly right gauge character.

B Mixing in the neutralino sector

In the MSSM, the four neutralinos $\tilde{\chi}_i^0$ ($i = 1, 2, 3, 4$) are mixtures of the neutral $U(1)$ and $SU(2)$ gauginos, \tilde{B} and \tilde{W}^3 , and the higgsinos, \tilde{H}_1^0 and \tilde{H}_2^0 . The neutralino mass matrix in the $(\tilde{B}, \tilde{W}^3, \tilde{H}_1^0, \tilde{H}_2^0)$ basis,

$$\mathcal{M}_N = \begin{pmatrix} M_1 & 0 & -m_Z c_{\beta} s_W & m_Z s_{\beta} s_W \\ 0 & M_2 & m_Z c_{\beta} c_W & -m_Z s_{\beta} c_W \\ -m_Z c_{\beta} s_W & m_Z c_{\beta} c_W & 0 & -\mu \\ m_Z s_{\beta} s_W & -m_Z s_{\beta} c_W & -\mu & 0 \end{pmatrix} \quad (50)$$

is built up by the fundamental SUSY parameters: the $U(1)$ and $SU(2)$ gaugino masses M_1 and M_2 , the higgsino mass parameter μ , and $\tan \beta = v_2/v_1$ ($c_{\beta} = \cos \beta$, $s_W = \sin \theta_W$ etc.). In addition to the μ parameter, a non-trivial CP phase can also be attributed to the M_1 parameter:

$$M_1 = |M_1| e^{i\phi_1}, \quad (0 \leq \phi_1 < 2\pi). \quad (51)$$

Since the complex matrix \mathcal{M}_N is symmetric, one unitary matrix N is sufficient to rotate the gauge eigenstate basis $(\tilde{B}, \tilde{W}^3, \tilde{H}_1^0, \tilde{H}_2^0)$ to the mass eigenstate basis of the Majorana fields $\tilde{\chi}_i^0$

$$\text{diag}(m_{\tilde{\chi}_1^0}, m_{\tilde{\chi}_2^0}, m_{\tilde{\chi}_3^0}, m_{\tilde{\chi}_4^0}) = N^* \mathcal{M}_N N^\dagger, \quad (m_{\tilde{\chi}_1^0} < m_{\tilde{\chi}_2^0} < m_{\tilde{\chi}_3^0} < m_{\tilde{\chi}_4^0}). \quad (52)$$

The masses $m_{\tilde{\chi}_i^0}$ ($i = 1, 2, 3, 4$) can be chosen to be real and positive by a suitable definition of the unitary matrix N .

C Interaction Lagrangian and couplings

The interaction Lagrangian for the stop decay ($\tilde{t}_i \rightarrow \tilde{\chi}_j^0 t$) is,

$$\mathcal{L}_{t\tilde{t}\tilde{\chi}^0} = \tilde{\chi}_j^0 (a_{ij} P_L + b_{ij} P_R) t \tilde{t}_i^* + \text{h.c.}, \quad (53)$$

where $P_{L,R} = \frac{1}{2}(1 \mp \gamma_5)$. The couplings are given by,

$$a_{ij} = -\frac{e}{\sqrt{2} s_W c_W} \mathcal{R}_{i1}^{\tilde{t}} \left(\frac{1}{3} s_W N_{j1}^* + c_W N_{j2}^* \right) - Y_t \mathcal{R}_{i2}^{\tilde{t}} N_{j4}^*, \quad (54)$$

$$b_{ij} = \frac{2\sqrt{2} e}{3c_W} \mathcal{R}_{i2}^{\tilde{t}} N_{j1} - Y_t \mathcal{R}_{i1}^{\tilde{t}} N_{j4}, \quad (55)$$

where $\mathcal{R}_{ij}^{\tilde{t}}$ are the entries of stop mixing matrix, Eq. (45), and N_{ij} are the entries of the neutralino mixing matrix, Eq. (52). The top Yukawa coupling is given by,

$$Y_t = \frac{e m_t}{\sqrt{2} m_W s_W \sin \beta}. \quad (56)$$

The interaction Lagrangian for the neutralino decay ($\tilde{\chi}_j^0 \rightarrow \tilde{\ell}\ell$) is,

$$\mathcal{L}_{\ell\tilde{\ell}\tilde{\chi}^0} = g f_{Lj}^\ell \bar{\ell} P_R \tilde{\chi}_j^0 \tilde{\ell}_L + g f_{Rj}^\ell \bar{\ell} P_L \tilde{\chi}_j^0 \tilde{\ell}_R + \text{h.c.} \quad (57)$$

where $g = e/\sin \theta_W$. The couplings are given by,

$$f_{Lj}^\ell = \frac{1}{\sqrt{2}} (\tan \theta_W N_{j1} + N_{j2}), \quad (58)$$

$$f_{Rj}^\ell = -\sqrt{2} \tan \theta_W N_{j1}^*, \quad (59)$$

$$(60)$$

D Amplitude squared including full spin correlations

D.1 Neutralino production $\tilde{t}_1 \rightarrow \tilde{\chi}_j^0 t$

Here we give the analytic expression for the neutralino production density matrix:

$$|M(\tilde{t}_1 \rightarrow \tilde{\chi}_j^0 t)|^2 = P(\tilde{\chi}_j^0 t) + \Sigma_P^a(\tilde{\chi}_j^0) + \Sigma_P^b(t) + \Sigma_P^{ab}(\tilde{\chi}_j^0 t), \quad (61)$$

whose spin-independent contribution reads

$$P(\tilde{\chi}_j^0 t) = (|a_{1j}|^2 + |b_{1j}|^2)(p_t p_{\tilde{\chi}_j^0}) - 2m_t m_{\tilde{\chi}_j^0} \text{Re}(a_{1j} b_{1j}^*), \quad (62)$$

where p_t and $p_{\tilde{\chi}_k^0}$ denote the four-momenta of the t -quark and the neutralino $\tilde{\chi}_k^0$. The coupling constants a_{ij} and b_{ij} are shown in Eq. (54,55) and by substituting the explicit matrix elements of Eq. (45) we can show the specific parameter dependence [59],

$$\begin{aligned} |a_{1j}|^2 + |b_{1j}|^2 &= \\ &= \cos^2 \theta_{\tilde{t}} \left(\frac{e^2}{2s_W^2 c_W^2} \left| \frac{1}{3} s_W N_{j1} + c_W N_{j2} \right|^2 + Y_t^2 |N_{j4}|^2 \right) + \sin^2 \theta_{\tilde{t}} \left(\frac{8e^2}{9c_W^2} |N_{j1}|^2 + Y_t^2 |N_{j4}|^2 \right) \\ &+ 2 \sin \theta_{\tilde{t}} \cos \theta_{\tilde{t}} Y_t \left(\frac{e}{\sqrt{2} s_W c_W} \text{Re} \left[e^{i\phi_{\tilde{t}}} \left(\frac{1}{3} s_W N_{j1}^* + c_W N_{j2}^* \right) N_{j4} \right] - \frac{2\sqrt{2} e}{3c_W} \text{Re} [e^{-i\phi_{\tilde{t}}} N_{j1} N_{j4}^*] \right). \end{aligned} \quad (63)$$

$$\begin{aligned} \text{Re} [a_{1j} b_{1j}^*] &= \cos^2 \theta_{\tilde{t}} \frac{e}{\sqrt{2} s_W c_W} Y_t \text{Re} \left[\left(\frac{1}{3} s_W N_{j1}^* + c_W N_{j2}^* \right) N_{j4} \right] + \sin^2 \theta_{\tilde{t}} \frac{2\sqrt{2} e}{3c_W} Y_t \text{Re} [N_{j4}^* N_{j1}] \\ &+ \sin \theta_{\tilde{t}} \cos \theta_{\tilde{t}} \left(Y_t^2 \text{Re} [e^{-i\phi_{\tilde{t}}} N_{j4}^{*2}] - \frac{2}{3} \frac{e^2}{s_W c_W^2} \text{Re} \left[e^{i\phi_{\tilde{t}}} \left(\frac{1}{3} s_W N_{j1}^* + c_W N_{j2}^* \right) N_{j1} \right] \right). \end{aligned} \quad (64)$$

The spin-dependent terms that depend on individual spin contributions are T-even and are given by,

$$\Sigma_P^a(\tilde{\chi}_j^0) = (|b_{ij}|^2 - |a_{ij}|^2) m_{\tilde{\chi}_j^0} (p_t s^a(\tilde{\chi}_j^0)), \quad (65)$$

$$\Sigma_P^b(t) = (|b_{ij}|^2 - |a_{ij}|^2) m_t (p_{\tilde{\chi}_j^0} s^b(t)), \quad (66)$$

where $s^a(\tilde{\chi}_j^0)$ ($s^b(t)$) denote the spin-basis vectors of the neutralino $\tilde{\chi}_j^0$ (t -quark). Again the coupling constants can be expanded as,

$$\begin{aligned} |b_{1j}|^2 - |a_{1j}|^2 &= \\ &= \cos^2 \theta_{\tilde{t}} \left(Y_t^2 |N_{j4}|^2 - \frac{e^2}{2s_W^2 c_W^2} \left| \frac{1}{3} s_W N_{j1} + c_W N_{j2} \right|^2 \right) + \sin^2 \theta_{\tilde{t}} \left(\frac{8e^2}{9c_W^2} |N_{j1}|^2 - Y_t^2 |N_{j4}|^2 \right) \\ &- 2 \sin \theta_{\tilde{t}} \cos \theta_{\tilde{t}} Y_t \left(\frac{e}{\sqrt{2} s_W c_W} \text{Re} \left[e^{i\phi_{\tilde{t}}} \left(\frac{1}{3} s_W N_{j1}^* + c_W N_{j2}^* \right) N_{j4} \right] + \frac{2\sqrt{2} e}{3c_W} \text{Re} [e^{-i\phi_{\tilde{t}}} N_{j1} N_{j4}^*] \right). \end{aligned} \quad (67)$$

The terms that depend simultaneously on the spin of the top quark and of the neutralino can be split into T-even, $\Sigma_{P,even}^{ab}(\tilde{\chi}_j^0 t)$, and T-odd, $\Sigma_{P,odd}^{ab}(\tilde{\chi}_j^0 t)$. The T-even contributions are as follows,

$$\begin{aligned} \Sigma_{P,even}^{ab}(\tilde{\chi}_j^0 t) &= 2 \text{Re}(a_{ij} b_{ij}^*) [(s^a(\tilde{\chi}_j^0) p_t)(s^b(t) p_{\tilde{\chi}_j^0}) - (p_t p_{\tilde{\chi}_j^0})(s^a(\tilde{\chi}_j^0) s^b(t))] \\ &+ m_t m_{\tilde{\chi}_j^0} (s^a(\tilde{\chi}_j^0) s^b(t)) (|a_{ij}|^2 + |b_{ij}|^2). \end{aligned} \quad (68)$$

The T-odd contributions that generate the triple product correlations that we are interested in are,

$$\Sigma_{P,odd}^{ab}(\tilde{\chi}_j^0 t) = -g^2 \text{Im}(a_{ij} b_{ij}^*) f_4^{ab}, \quad (69)$$

where the T-odd kinematical factor is given by,

$$f_4^{ab} = \epsilon_{\mu\nu\rho\sigma} s^{a,\mu}(\tilde{\chi}_j^0) p_{\tilde{\chi}_j^0}^\nu s^{b,\rho}(t) p_t^\sigma. \quad (70)$$

Sec.2.2 explains how this epsilon product generates the triple product observable. We again expand the coupling constant to see the functional dependence,

$$\begin{aligned} \text{Im}[a_{1j} b_{1j}^*] &= \cos^2 \theta_{\tilde{t}} \frac{e}{\sqrt{2} s_W c_W} Y_t \text{Im} \left[\left(\frac{1}{3} s_W N_{j1}^* + c_W N_{j2}^* \right) N_{j4}^* \right] + \sin^2 \theta_{\tilde{t}} \frac{2\sqrt{2} e}{3 c_W} Y_t \text{Im}[N_{j4}^* N_{j1}^*] \\ &+ \sin \theta_{\tilde{t}} \cos \theta_{\tilde{t}} \left(Y_t^2 \text{Im} [e^{-i\phi_{\tilde{t}}} N_{j4}^{*2}] - \frac{2}{3} \frac{e^2}{s_W c_W^2} \text{Im} \left[e^{i\phi_{\tilde{t}}} \left(\frac{1}{3} s_W N_{j1}^* + c_W N_{j2}^* \right) N_{j1}^* \right] \right). \end{aligned} \quad (71)$$

D.2 Neutralino decay $\tilde{\chi}_2^0 \rightarrow \tilde{\ell}_R^+ \ell^-$

We provide analytical expressions for the 2-body decay of the $\tilde{\chi}_2^0$ into a $\tilde{\ell}_R^+$ and the final-state ℓ^- :

$$D(\tilde{\chi}_2^0) = \frac{g^2}{4} |f_{L2}^l|^2 \{m_{\tilde{\chi}_2^0}^2 - m_{\tilde{\ell}_R}^2\}. \quad (72)$$

The spin-dependent contribution is T-even and reads:

$$\Sigma_D^a(\tilde{\chi}_2^0) = \frac{g^2}{2} |f_{L2}^l|^2 m_{\tilde{\chi}_2^0} \{s^a(\tilde{\chi}_2^0) p_{\ell^-}\}. \quad (73)$$

D.3 Top decay $t \rightarrow W^+ b$

We provide analytical expressions for the 2-body decay of the top quark into a W -boson and the final-state bottom quark:

$$D(t) = \frac{g^2}{4} \{m_t^2 - 2m_W^2 + \frac{m_t^4}{m_W^2}\}. \quad (74)$$

The spin-dependent contribution is T-even and reads:

$$\Sigma_D^b(t) = -\frac{g^2}{2} m_t \{s^b(t) p_b\} + \frac{m_t^2 - m_W^2}{m_W^2} (s^b(t) p_W)\}. \quad (75)$$

References

- [1] O. Buchmueller *et al.*, “Likelihood Functions for Supersymmetric Observables in Frequentist Analyses of the CMSSM and NUHM1,” [arXiv:0907.5568](#) [[hep-ph](#)].
- [2] A. G. Cohen, D. B. Kaplan, and A. E. Nelson, “Progress in electroweak baryogenesis,” *Ann. Rev. Nucl. Part. Sci.* **43** (1993) 27–70, [arXiv:hep-ph/9302210](#).
- [3] M. B. Gavela, P. Hernandez, J. Orloff, O. Pene, and C. Quimbay, “Standard model CP violation and baryon asymmetry. Part 2: Finite temperature,” *Nucl. Phys.* **B430** (1994) 382–426, [arXiv:hep-ph/9406289](#).
- [4] V. A. Rubakov and M. E. Shaposhnikov, “Electroweak baryon number non-conservation in the early universe and in high-energy collisions,” *Usp. Fiz. Nauk* **166** (1996) 493–537, [arXiv:hep-ph/9603208](#).
- [5] S. Dimopoulos and D. W. Sutter, “The Supersymmetric flavor problem,” *Nucl. Phys.* **B452** (1995) 496–512, [arXiv:hep-ph/9504415](#).
- [6] T. Ibrahim and P. Nath, “CP violation from standard model to strings,” *Rev. Mod. Phys.* **80** (2008) 577–631, [arXiv:0705.2008](#) [[hep-ph](#)].
- [7] J. R. Ellis, J. S. Lee, and A. Pilaftsis, “Electric Dipole Moments in the MSSM Reloaded,” *JHEP* **10** (2008) 049, [arXiv:0808.1819](#) [[hep-ph](#)].
- [8] Y. Kizukuri and N. Oshimo, “The Neutron and electron electric dipole moments in supersymmetric theories,” *Phys. Rev.* **D46** (1992) 3025–3033.
- [9] T. Ibrahim and P. Nath, “The neutron and the lepton EDMs in MSSM, large CP violating phases, and the cancellation mechanism,” *Phys. Rev.* **D58** (1998) 111301, [arXiv:hep-ph/9807501](#).
- [10] T. Ibrahim and P. Nath, “Large CP phases and the cancellation mechanism in EDMs in SUSY, string and brane models,” *Phys. Rev.* **D61** (2000) 093004, [arXiv:hep-ph/9910553](#).
- [11] M. Brhlik, G. J. Good, and G. L. Kane, “Electric dipole moments do not require the CP-violating phases of supersymmetry to be small,” *Phys. Rev.* **D59** (1999) 115004, [arXiv:hep-ph/9810457](#).
- [12] S. Abel, S. Khalil, and O. Lebedev, “EDM constraints in supersymmetric theories,” *Nucl. Phys.* **B606** (2001) 151–182, [arXiv:hep-ph/0103320](#).
- [13] R. L. Arnowitt, B. Dutta, and Y. Santoso, “SUSY phases, the electron electric dipole moment and the muon magnetic moment,” *Phys. Rev.* **D64** (2001) 113010, [arXiv:hep-ph/0106089](#).

- [14] Y. Li, S. Profumo, and M. Ramsey-Musolf, “A Comprehensive Analysis of Electric Dipole Moment Constraints on CP-violating Phases in the MSSM,” [arXiv:1006.1440](#) [hep-ph].
- [15] J. S. Lee *et al.*, “CPsuperH: A computational tool for Higgs phenomenology in the minimal supersymmetric standard model with explicit CP violation,” *Comput. Phys. Commun.* **156** (2004) 283–317, [arXiv:hep-ph/0307377](#).
- [16] J. S. Lee, M. Carena, J. Ellis, A. Pilaftsis, and C. E. M. Wagner, “CPsuperH2.0: an Improved Computational Tool for Higgs Phenomenology in the MSSM with Explicit CP Violation,” *Comput. Phys. Commun.* **180** (2009) 312–331, [arXiv:0712.2360](#) [hep-ph].
- [17] F. Deppisch and O. Kittel, “Probing SUSY CP Violation in Two-Body Stop Decays at the LHC,” [arXiv:0905.3088](#) [hep-ph].
- [18] S. Kraml, “CP violation in SUSY,” [arXiv:0710.5117](#) [hep-ph].
- [19] V. D. Barger, T. Han, T.-J. Li, and T. Plehn, “Measuring CP Violating Phases at a Future Linear Collider,” *Phys. Lett.* **B475** (2000) 342–350, [arXiv:hep-ph/9907425](#).
- [20] J. L. Kneur and G. Moultaka, “Phases in the gaugino sector: Direct reconstruction of the basic parameters and impact on the neutralino pair production,” *Phys. Rev.* **D61** (2000) 095003, [arXiv:hep-ph/9907360](#).
- [21] O. Kittel, “SUSY CP phases and asymmetries at colliders,” [arXiv:0904.3241](#) [hep-ph].
- [22] S. Hesselbach, “CP Violation in SUSY Particle Production and Decay,” [arXiv:0709.2679](#) [hep-ph].
- [23] P. Langacker, G. Paz, L.-T. Wang, and I. Yavin, “A T-odd observable sensitive to CP violating phases in squark decay,” *JHEP* **07** (2007) 055, [arXiv:hep-ph/0702068](#).
- [24] J. Ellis, F. Moortgat, G. Moortgat-Pick, J. M. Smillie, and J. Tattersall, “Measurement of CP Violation in Stop Cascade Decays at the LHC,” *Eur. Phys. J.* **C60** (2009) 633–651, [arXiv:0809.1607](#) [hep-ph].
- [25] K. Kiers, A. Szykman, and D. London, “CP violation in supersymmetric theories: stop(2) \rightarrow stop(1) tau- tau+,” *Phys. Rev.* **D74** (2006) 035004, [arXiv:hep-ph/0605123](#).
- [26] A. Bartl, E. Christova, K. Hohenwarter-Sodek, and T. Kernreiter, “Triple product correlations in top squark decays,” *Phys. Rev.* **D70** (2004) 095007, [arXiv:hep-ph/0409060](#).
- [27] A. Bartl, E. Christova, K. Hohenwarter-Sodek, and T. Kernreiter, “CP asymmetries in scalar bottom quark decays,” *JHEP* **11** (2006) 076, [arXiv:hep-ph/0610234](#).

- [28] F. F. Deppisch and O. Kittel, “CP violation in sbottom decays,” *JHEP* **06** (2010) 067, [arXiv:1003.5186 \[hep-ph\]](#).
- [29] G. Moortgat-Pick, K. Rolbiecki, J. Tattersall, and P. Wienemann, “Probing CP Violation with and without Momentum Reconstruction at the LHC,” *JHEP* **01** (2010) 004, [arXiv:0908.2631 \[hep-ph\]](#).
- [30] D. Atwood, S. Bar-Shalom, G. Eilam, and A. Soni, “CP violation in top physics,” *Phys. Rept.* **347** (2001) 1–222, [arXiv:hep-ph/0006032](#).
- [31] G. A. Moortgat-Pick, H. Fraas, A. Bartl, and W. Majerotto, “Polarization and spin effects in neutralino production and decay,” *Eur. Phys. J.* **C9** (1999) 521–534, [arXiv:hep-ph/9903220](#).
- [32] H. E. Haber, “Spin formalism and applications to new physics searches,” [arXiv:hep-ph/9405376](#).
- [33] J. S. Schwinger, “The theory of quantized fields. I,” *Phys. Rev.* **82** (1951) 914–927.
- [34] J. S. Schwinger, “The theory of quantized fields. II,” *Phys. Rev.* **91** (1953) 713–728.
- [35] K. Kawagoe, M. M. Nojiri, and G. Polesello, “A new SUSY mass reconstruction method at the CERN LHC,” *Phys. Rev.* **D71** (2005) 035008, [arXiv:hep-ph/0410160](#).
- [36] B. K. Gjelsten, D. J. Miller, 2, and P. Osland, “Measurement of SUSY masses via cascade decays for SPS 1a,” *JHEP* **12** (2004) 003, [arXiv:hep-ph/0410303](#).
- [37] M. M. Nojiri, G. Polesello, and D. R. Tovey, “Proposal for a new reconstruction technique for SUSY processes at the LHC,” [arXiv:hep-ph/0312317](#).
- [38] M. M. Nojiri, G. Polesello, and D. R. Tovey, “A hybrid method for determining SUSY particle masses at the LHC with fully identified cascade decays,” *JHEP* **05** (2008) 014, [arXiv:0712.2718 \[hep-ph\]](#).
- [39] H.-C. Cheng, J. F. Gunion, Z. Han, G. Marandella, and B. McElrath, “Mass Determination in SUSY-like Events with Missing Energy,” *JHEP* **12** (2007) 076, [arXiv:0707.0030 \[hep-ph\]](#).
- [40] H.-C. Cheng, J. F. Gunion, Z. Han, and B. McElrath, “Accurate Mass Determinations in Decay Chains with Missing Energy: II,” [arXiv:0905.1344 \[hep-ph\]](#).
- [41] D. Casadei, R. Djilibaev, and R. Konoplich, “Reconstruction of stop quark mass at the LHC,” [arXiv:1006.5875 \[hep-ph\]](#).
- [42] A. J. Barr and C. G. Lester, “A Review of the Mass Measurement Techniques proposed for the Large Hadron Collider,” [arXiv:1004.2732 \[hep-ph\]](#).

- [43] G. Brooijmans *et al.*, “New Physics at the LHC. A Les Houches Report: Physics at TeV Colliders 2009 - New Physics Working Group,” [arXiv:1005.1229](#) [hep-ph].
- [44] W. Porod, “SPHeno, a program for calculating supersymmetric spectra, SUSY particle decays and SUSY particle production at e+ e- colliders,” *Comput. Phys. Commun.* **153** (2003) 275–315, [arXiv:hep-ph/0301101](#).
- [45] M. Bahr *et al.*, “Herwig++ Physics and Manual,” [arXiv:0803.0883](#) [hep-ph].
- [46] M. Bahr *et al.*, “Herwig++ 2.3 Release Note,” [arXiv:0812.0529](#) [hep-ph].
- [47] A. D. Martin, W. J. Stirling, R. S. Thorne, and G. Watt, “Update of Parton Distributions at NNLO,” *Phys. Lett.* **B652** (2007) 292–299, [arXiv:0706.0459](#) [hep-ph].
- [48] A. Buckley *et al.*, “Rivet user manual,” [arXiv:1003.0694](#) [hep-ph].
- [49] B. M. Waugh *et al.*, “HZTool and Rivet: Toolkit and framework for the comparison of simulated final states and data at colliders,” [arXiv:hep-ph/0605034](#).
- [50] M. Cacciari and G. P. Salam, “Dispelling the N^3 myth for the k_t jet-finder,” *Phys. Lett.* **B641** (2006) 57–61, [arXiv:hep-ph/0512210](#).
- [51] M. Cacciari, G. P. Salam, and G. Soyez, “The anti- k_t jet clustering algorithm,” *JHEP* **04** (2008) 063, [arXiv:0802.1189](#) [hep-ph].
- [52] **The ATLAS Collaboration**, G. Aad *et al.*, “Expected Performance of the ATLAS Experiment - Detector, Trigger and Physics,” [arXiv:0901.0512](#) [hep-ex].
- [53] J. Alwall *et al.*, “MadGraph/MadEvent v4: The New Web Generation,” *JHEP* **09** (2007) 028, [arXiv:0706.2334](#) [hep-ph].
- [54] K. Desch, J. Kalinowski, G. Moortgat-Pick, K. Rolbiecki, and W. J. Stirling, “Combined LHC / ILC analysis of a SUSY scenario with heavy sfermions,” *JHEP* **12** (2006) 007, [arXiv:hep-ph/0607104](#).
- [55] W. Beenakker, R. Hopker, and M. Spira, “PROSPINO: A program for the PROduction of Supersymmetric Particles In Next-to-leading Order QCD,” [arXiv:hep-ph/9611232](#).
- [56] W. Beenakker, R. Hopker, M. Spira, and P. M. Zerwas, “Squark and gluino production at hadron colliders,” *Nucl. Phys.* **B492** (1997) 51–103, [arXiv:hep-ph/9610490](#).
- [57] W. Beenakker, M. Kramer, T. Plehn, M. Spira, and P. M. Zerwas, “Stop production at hadron colliders,” *Nucl. Phys.* **B515** (1998) 3–14, [arXiv:hep-ph/9710451](#).
- [58] **Particle Data Group** Collaboration, C. Amsler *et al.*, “Review of particle physics,” *Phys. Lett.* **B667** (2008) 1.

- [59] K. Rolbiecki, J. Tattersall, and G. Moortgat-Pick, “Measuring the Stop Mixing Angle at the LHC,” [arXiv:0909.3196](https://arxiv.org/abs/0909.3196) [hep-ph].